Invited Centennial Article for American Mineralogist

Cancrinite-group minerals. Crystal-chemical description and properties under non-ambient conditions: A review

[1,2]G. Diego Gatta and [1]Paolo Lotti

[1]Dipartimento di Scienze della Terra, Università degli Studi di Milano, Via Botticelli 23, I-20133 Milano, Italy

[2]CNR - Istituto di Cristallografia, Sede di Bari, Via G. Amendola 122/o, I-70126 Bari, Italy

Abstract

This is a review of the thermal and compressional behavior of cancrinite-group minerals with a description of the mechanisms, at the atomic scale, that govern their (*P*,*T*)-induced structure evolution. The open-framework structure of this group of feldspathoids is characterized by the [CAN] topology, which contains large parallel channels (confined by 12-membered rings of tetrahedra), surrounded by columns of cages. At least two structural "subgroups" can be identified according to the nature of the constituents filling the cages, irrespective of the channel population. The minerals of the "cancrinite subgroup" show $[NaH_2O]^+$ clusters into the cages and those of the "davyne subgroup" contains $[CaCl]^+$ clusters. Beside a similar bulk compressibility and expansivity at room conditions for all the minerals of the group, a different elastic anisotropy, coupled with different deformation mechanisms of the tetrahedral framework, were found to be mainly controlled by the nature of the population filling the cages. The role played by the channel populations appear being secondary. These experimental findings allow us to provide a model of the structure evolution in response to the different cage content, *i.e.* NaH_2O^+ and $CaCl^+$.

The high-temperature studies of the hydrous members of the cancrinite subgroup reveal a slow dehydration process, often irreversible at the time-scale of the experiments and leading to quasi-anhydrous high-temperature forms which keep their crystallinity even up to 800-900 K (at room *P*). The experiments at high pressure on the cancrinite-group minerals show a high-*P* stability, at least up to 7-8 GPa (at room-*T*), which is quite surprising if we consider their microporous nature. The *P*-induced stability is the effect of a pronounced structural flexibility, which in turn is based mainly on tilting of rigid tetrahedra around O atoms that behave as hinges. The character and the mechanisms that govern the (*P*,*T*)-induced $P6_3$-to-$P6_3/m$ phase transition in the compounds of davyne subgroup are also discussed.

Keywords: Feldspathoids; cancrinite; davyne; vishnevite; balliranoite; temperature; pressure; elastic behavior; host-guest interactions; framework deformation.

Introduction

Feldspathoids are a loosely-defined class of minerals with a structure characterized by a three-dimensional framework of linked SiO_4 and AlO_4 (more rarely PO_4 or BeO_4) tetrahedra. This framework contains open cavities (in the form of channels and cages), usually occupied by cations (mainly Na^+, K^+, Ca^{2+}), anions (mainly CO_3^{2-}, SO_4^{2-}, Cl^-) and molecules (mainly H_2O). Compared with feldspars, the aluminosilicate feldspathoids are deficient in SiO_2. They occur in a wide variety of geological environments and conditions, from sedimentary to alkali-rich SiO_2-poor igneous rocks or metamorphic and metasomatic rocks, from crustal to upper mantle conditions. Some feldspathoids have been found in meteorites (*e.g.* in carbonaceous chondrites, Grossman 1980).

This class of minerals is the major host of C, S or Cl structurally incorporated in silicates. The structural diversity of feldspathoids is reflected by their complex systematics with at least three different principal families: analcime-leucite (*e.g*. Gatta et al. 2006, 2008a), nepheline-kalsilite (*e.g*. Gatta and Angel 2007; Gatta et al. 2010, 2011) and cancrinite-sodalite (*e.g*. Gatta et al. 2012a; Lotti et al. 2012; Löns and Schulz 1967). Minerals of the melilite family (*i.e*. melilite *sensu stricto*, gehlenite and akermanite) are also considered as feldspathoids (Edgar 1984). A comprehensive overview on the structures of feldspathoids is reported in Merlino (1984).

When compared to other silicates, only a modest number of experiments have been devoted to cancrinite-group minerals at high pressure or high temperature. Some *in situ* experiments at high temperature on the most important member of the group (*i.e*. cancrinite *sensu stricto*) actually provided conflicting results (Hassan 1996a, 1996b; Sirbescu and Jenkins 1999; Hassan et al. 2006; Isupova et al. 2010; Gatta et al. 2014). A full characterization of the phase stability fields of cancrinite-group minerals and of the reactions at the field boundaries is still missing or limited to restricted experimental conditions (*e.g.* Sirbescu and Jenkins 1999 and references therein). To overcome this deficiency, we have recently conducted a series of *in situ* experiments on the behavior of cancrinite-group minerals at non-ambient conditions (*i.e.* high pressure, low and high

temperature), as part of a wider research project on microporous materials at extreme conditions (*e.g.* Gatta et al. 2012a, 2013a, 2013b; 2014; Lotti et al. 2012, 2014a, 2014b; Lotti 2014).

The aim of this manuscript is a synthesis of previously published data on the behavior of cancrinite-group minerals at non-ambient conditions, in order to provide a model of their thermo-elastic behavior and of the main deformation mechanisms, at the atomic scale, in response to the applied temperature (*T*) and pressure (*P*). In particular, the role played by the different extraframework constituents is reviewed and discussed.

Crystal chemistry of cancrinite-group minerals

Minerals of the cancrinite group share the tetrahedral [CAN] framework-type, built by the stacking of layers made by unconnected single six-membered rings of tetrahedra (hereafter S6R's) occupying A or B positions, respectively, according to an ···AB(A)··· sequence (Gies et al. 1999; Baerlocher et al. 2007). Each S6R is connected to three rings in adjacent layers, giving rise to the three-dimensional framework (Figure 1, see also http://www.iza-structure.org/databases/Catalog/ABC_6.pdf). The [CAN] framework contains columns of base-sharing cages (*i.e*. *can* units or cancrinite cages), where the bases correspond to the single six-membered rings perpendicular to the **c**-axis (S6R⊥[0001], Figure 1). These columns surround parallel channels to [0001] and are confined by twelve-membered rings of tetrahedra (12R) (Figure 1). The framework can also be described as made of double *zigzag* chains of tetrahedra (*dzc* units, Smith 2000), made by edge-sharing four-membered rings (S4R), running along the **c**-axis, which border 6R-windows∠[0001] linking cages and channels (Figure 1). The topological symmetry of the [CAN] framework is $P6_3/mmc$ (Baerlocher et al. 2007). Overall, materials with [CAN] framework type are considered as "microporous materials" (*sensu* Rouquerol et al. 1994), having cavities with free diameters shorter than 2 nm.

Twelve mineralogical species sharing the [CAN] topology have so far been reported (Bonaccorsi and Merlino 2005; Pekov et al. 2011a) (Table 1) and eleven of them show an aluminosilicate framework; the only exception is tiptopite, with a P/Be-framework (Table 1; Peacor et al. 1987). In cancrinite-group minerals, the Si/Al-distribution of the $(Al_6Si_6O_{24})^{6-}$-framework is fully ordered, with a lowering of the symmetry from $P6_3/mmc$ to $P6_3$ (or $P6_3/m$), with only rare exceptions (Rastsvetaeva et al. 2007; Ogorodova et al. 2009). In this group of minerals, the extraframework population can be subdivided according to the structural voids, namely: 1) the *can* cages and 2) the 12R-channels. Only two mutually exclusive configurations of the cage constituents are shown by the aluminosilicate cancrinite-group minerals: the first is given by the repetition of $[Na{\cdot}H_2O]^+$ clusters, so that chains along the columns of *can* units arise, and, similarly, the second configuration is represented by chains of $[Ca{\cdot}Cl]^+$ clusters (Figure 2). In contrast, a complex chemical variability is shown by the 12R-channel population, made by cations, anions and molecular components, though a general scheme can be extrapolated. Na^+ is always the prevailing cation, it can be partially replaced by Ca^{2+} and K^+ in one or two crystallographic sites close to the channel walls (Figure 3); a more complex positional disorder was also reported (*e.g.* Gatta et al. 2013a). Nevertheless, a similar bonding environment of cations can be described, with 4-5 bonds to the framework oxygen atoms on the wall-side and a variable coordination with the anionic groups or molecules on the other side. Anions and molecules occupy the center of the channel (Figure 3), often in mutually-exclusive split positions, so that several possible configurations can occur within the same channel. These configurations can be ordered, leading to superstructures (see next section). The most common anionic and molecular species in cancrinite-group minerals are: CO_3^{2-}, SO_4^{2-}, Cl^-, $C_2O_4^{2-}$, PO_4^{3-}, OH^- and H_2O. The most abundant anion is conventionally used as "species-defining criterion" (Bonaccorsi and Merlino 2005; Pekov et al. 2011a).

For a comparative and comprehensive analysis of the H*P*-H*T* crystal-chemistry of this mineral group, two "subgroups" can be defined: the "cancrinite subgroup", showing chains of

139 $[Na \cdot H_2O]^+$ clusters, and the "davyne subgroup", with $[Ca \cdot Cl]^+$ chains (Figure 2). In the next
140 sections we describe the crystallochemical features and the occurrences of these isotypic minerals.

141

142 *- The "cancrinite subgroup"*

143 In the structural cages of this subgroup, the Na^+ site is slightly displaced from the
144 S6R⊥[0001]-plane, with a stronger bond to one of the neighboring H_2O-oxygen sites, positioned
145 out of the 3-fold axis approximately at the cage center (Figure 2). Therefore, each H_2O molecule
146 shows a shorter bond to one Na^+ cation and a longer one to the other Na-neighbor, which, in turn, is
147 strongly bonded to the next H_2O molecule (Figure 2). Similarly, Na^+ shows shorter bonds to the
148 three O2 oxygen sites than those to the three O1 sites. As a consequence, a significant deviation
149 from the hexagonal shape is shown by the S6R⊥[0001] (Figure 1). The Na^+ coordination
150 environment can, therefore, be described by a first tetrahedral shell (3·O2 + Ow′) along with a
151 second larger tetrahedral one (3·O1 + Ow″), giving rise to a distorted ditrigonal bipyramid (C.N. =
152 4 + 4).

153 Cancrinite *sensu stricto* $[(Na,Ca)_6(CO_3)_{1.4\text{-}1.7}][NaH_2O]_2[Al_6Si_6O_{24}]$ (Table 1; Bonaccorsi and
154 Merlino 2005) is, by far, the most widespread mineral of the group. Its crystal structure was first
155 solved by Pauling (1930), and then refined by Jarchow (1965). Cancrinite contains CO_3^{2-} as main
156 anionic component in the channel voids. The CO_3^{2-} groups occupy the center of the channel in two
157 mutually exclusive and iso-oriented configurations, for which the neighboring cations face an edge
158 of the triangular anionic group, giving rise to two bonds to the closer oxygen atoms (Figure 3). Due
159 to the resulting short C-C contacts, not all the sub-cells can be occupied by the carbonate anions,
160 with positional order/disorder leading also to superstructures (*e.g.* Foit et al. 1973; Grundy and
161 Hassan 1982; Hassan and Buseck 1992).

Vishnevite $[(Na,K)_6(SO_4)][NaH_2O]_2[Al_6Si_6O_{24}]$ (Table 1; Hassan and Grundy 1984; Della Ventura et al. 2007) is the (SO_4^{2-})-dominant end-member. Two distinct configurations can be defined for the channel population. The first, with $[Na_3(SO_4)]^+$ clusters, is given by the Na^+ cations and sulfate tetrahedral groups at the center of the channel, for which the triangular basis is generally found to point a vertex toward the neighboring Na^+ atoms, so that a single $Na\text{-}O_{SO4}$ bond occurs (Figure 3). The second, with only Na and K sites bonded to the framework oxygens, is commonly associated to vacancies at the anionic sites (at the channel center), in order to avoid too short K-O bonds (Figure 3). A channel can be internally ordered. If there is an ordered distribution of these configurations among adjacent channels, a superstructure with a new unit-cell **a**-parameter, equal to $\sqrt{3}\mathbf{a}_{vish}$, arises. This gives rise to a new mineralogical species called pitiglianoite (Table 1; Merlino et al. 1991; Della Ventura et al. 2005; Bonaccorsi et al. 2007), which shares with vishnevite a common **c**-parameter.

Hydroxycancrinite (or "basic cancrinite") is the (OH^-)-dominant end-member of the cancrinite subgroup (Table 1) and is often reported as a synthetic product. In Nature, it is rare and usually represented by intermediate members of the cancrinite-hydroxycancrinite series in the peralkaline plutons of the Kola peninsula, Russia (Pekov et al. 2011a). Kyanoxalite is the $C_2O_4^{2-}$ member (Table 1). It is very rare in Nature; minerals of the cancrinite-kyanoxalite series have, up to now, been found only at the Lovozero alkaline pluton, Kola peninsula, Russia (Chukanov et al. 2010a; Olysych et al. 2011; Pekov et al. 2011a). Depmeierite is the PO_4^{3-}-dominant member of the cancrinite subgroup (Table 1) and has been reported only from Mt. Karnasurt, Kola peninsula, Russia (Pekov et al. 2011b).

Cancrisilite is the only member of the cancrinite group of minerals showing the framework enriched in Si^{4+}, with an ideal Si^{4+}:Al^{3+} ratio of 7:5 (Table 1). This leads to a disordered Si/Al-distribution in the tetrahedral framework, with an increase in symmetry from $P6_3$ to $P6_3mc$ (Ogorodova et al. 2009).

187

188 - *The "davyne subgroup"*

189 The davyne-subgroup minerals contain chains of alternating $[Ca{\cdot}Cl]^{+}$ clusters. The Ca^{2+} site
190 lies close to the S6R⊥[0001] "plane" (*i.e*. the cage basis) and is bonded to the three O2 and the
191 three O1 atoms, showing similar bond lengths (Figure 2). Therefore, only a small deviation from the
192 perfect hexagonal shape of the S6R⊥[0001] is observed in davyne-subgroup minerals (Figure 1).
193 The Cl^{-} anion is placed approximately at the center of the cage in three mutually exclusive positions
194 out of the 3-fold axis (Figure 2). Each Ca^{2+} cation is bonded to the two neighboring Cl^{-}, giving rise
195 to a slightly distorted hexagonal bipyramidal coordination shell (C.N. = 8).

196 Davyne $[(Na,K)_6(SO_4,Cl)][CaCl]_2[Al_6Si_6O_{24}]$ (Table 1; Hassan and Grundy 1990;
197 Bonaccorsi et al. 1990; Gatta et al. 2013a; Lotti et al. 2014a) and balliranoite $[(Na,Ca)_6(CO_3)_{1.4\text{-}}$
198 $_{1.7}][CaCl]_2[Al_6Si_6O_{24}]$ (Table 1; Chukanov et al. 2010b; Gatta et al. 2013b; Lotti et al. 2014b) are
199 the (SO_4^{2-},Cl^{-})- and CO_3^{2-}-end-members, respectively, and show a channel configuration analogous
200 to that of vishnevite (for davyne) and cancrinite (for balliranoite) (Figure 3). In microsommite
201 (Table 1; Bonaccorsi et al. 2001), the ordered distribution along the channel of SO_4^{2-} groups and
202 vacancies at the anionic sites (at the channel center) leads to a superstructure similar to that shown
203 by pitiglianoite ($\mathbf{a}_{MIC} = \sqrt{3}\cdot\mathbf{a}_{DAV}$, $\mathbf{c}_{MIC} = \mathbf{c}_{DAV}$), whereas in the pure Cl^{-}-end-member, quadridavyne
204 (Table 1; Bonaccorsi et al. 1994), a different kind of superstructure occurs, with $\mathbf{a}_{QUA} = 2\cdot\mathbf{a}_{DAV}$ and
205 $\mathbf{c}_{QUA} = \mathbf{c}_{DAV}$.

206

207 - *Natural occurrence of cancrinite-group minerals*

208 Cancrinite-group minerals are typical of silica-undersaturated rocks and rich in alkalis,
209 particularly Na. They are commonly related to alkaline magmatism (Deer et al. 2004). Cancrinite-

group minerals are widespread both in intrusive igneous rocks, such as nepheline syenites, and in extrusive rocks, such as phonolites. In addition, they can be found in metasomatic environments related to alkaline magmas and/or limestone wallrocks.

Pekov et al. (2011a) suggested the distinction between cancrinite and davyne subgroups to have also a genetic relevance, being the minerals of the first subgroup most commonly found in intrusive environments and those of the second subgroup in effusive and metasomatic settings. Cancrinite-subgroup minerals are widespread in intrusive alkaline magmatic complexes, where they can crystallize: 1) as primary phases during the late-magmatic stage, typical of vein- and dyke-intrusions or pegmatites (*e.g*. Erd and Czamanske 1983; Deer et al. 2004), or 2) as secondary phases from hydrothermal alteration of pre-existing minerals (*e.g*. Bell et al. 1996; Sindern and Kramm 2000; Fall et al. 2007).

The davyne-subgroup minerals can be typically found in effusive and metasomatic environments, especially in lithic blocks within pyroclastic, tephritic and pumice deposits. They generally occur in cavities of skarn-like rocks, likely formed as thermal metamorphic and metasomatic products, around the magmatic chamber walls (*e.g.* Deer et al. 2004; Fulignati et al. 2005; Sapozhnikov 2010; Harlow and Bender 2013).

Description of the compressional and expansion behavior: the equations of state

For a comparative analysis of the elastic behavior of cancrinite-group minerals, their volume compressibility and expansivity parameters are here determined by fitting the experimental unit-cell data to *P*-*V* and *T*-*V* equations of state. The isothermal Birch-Murnaghan equation of state (BM-EoS) was adopted for the high-pressure data. The BM-EoS is based on the assumption that the strain energy in a solid can be described as a Taylor series in the Eulerian finite strain,

$f_e = [(V_0/V)^{2/3} - 1]/2$ (Birch 1947; Angel 2000).

In the H*P*-studies of cancrinite-group minerals (Lotti et al. 2012, 2014a, 2014b; Lotti 2014), the polynomial truncated to third order in energy (III-BM EoS) was used, with the following form:

$$P = 3K_0 f_e(1 + 2f_e)^{5/2} [1 + 3/2(K' - 4)f_e],$$

where K_0 is the isothermal bulk modulus, *i.e.* the inverse of the volume compressibility:

$$K_0 = 1/\beta_V = -V\cdot(\partial P/\partial V),$$

and *K'* is its pressure-derivative (*i.e.* $K' = \partial K_0/\partial P$). When a BM-EoS is truncated to second order in energy, $K' = 4$ is implied. "Linearized" BM-equations of state, for which the cube of a linear parameter (*e.g.* unit-cell edge) replaces the volume, were adopted to fit the experimental *l*-*P* data and, therefore, to describe the anisotropy of the elastic behavior. The obtained "linear-K_0" (Angel 2000) is one third of the inverse of the linear volume compressibility: $K_{l0} = 1/3\beta_l$.

The elastic behavior in the low-*T* range (ca. 110-293 K) was described by Gatta et al. (2012a, 2013a, 2013b) fitting the experimental data with an equation directly derived from the thermodynamic definition of the thermal expansion coefficient:

$$\alpha_V = V^{-1}(\partial V/\partial T),\ V(T) = V_0 e^{[\alpha_V (T-T_0)]},$$

assuming a constant α_V value due to the low number of the experimental data. The high-temperature elastic behavior of cancrinite was described by Gatta et al. (2014) with a modified second-order polynomial equation proposed by Berman (1988) and implemented in the EOSFIT7 software (Angel et al. 2014):

$$V(T) = V_0[1 + a_0(T-T_0) - 2(10a_0 + a_1)(T^{1/2} - T_0^{1/2})],$$

where $\alpha_V = a_0 + a_1(T - T_0)$, a_0 and a_1 are two refinable parameters.

255 **Compressional behavior of the cancrinite-group minerals**

256 The *P*-induced evolution of the unit-cell parameters of the studied cancrinite-group minerals
257 is shown in Figure 4, and the elastic parameters, refined from BM-EoS fits, are listed in Table 2.
258 These parameters show that all the studied minerals have similar bulk muduli at room conditions,
259 where the refined K_0 values (~47 GPa) fall in the range so far reported for open-framework silicates
260 (Gatta 2008, 2010; Gatta and Lee 2014). Moreover, all the members of the group share the same
261 elastic anisotropy scheme, where the most compressible direction, along the **c** crystallographic axis,
262 corresponds to the stacking of S6R-layers (Figure 1). Besides the similar anisotropy scheme, the
263 calculated K_a:K_c ratios (Table 2) suggest a different behavior for the cancrinite- and the davyne-
264 subgroup minerals, with elastic anisotropy more pronounced in the formers.

265 If the *P*-induced elastic response of davyne and balliranoite is virtually identical within
266 estimated standard deviations (Figure 4; Table 2; Lotti et al. 2014a,b), a comparison of the
267 cancrinite and vishnevite behaviors shows a different scenario. Vishnevite clearly shows a
268 significant increase in compressibility, related to a structural re-arrangement of the channel
269 population (Lotti 2014) at $P > 3.43$ GPa. In cancrinite, an apparent softening is observed at higher
270 pressures ($P > 4.62$ GPa; Lotti et al. 2012) by the evolution of the unit-cell parameters with *P*, but
271 without any significant change in the evolution of structural parameters at the atomic scale. For both
272 cancrinite and vishnevite, the change in the elastic behavior at high pressure leads to an increase of
273 the elastic anisotropy (Table 2). Nevertheless, the elastic parameters reported in Table 2 suggest that
274 the minerals of this subgroup share the same bulk compressibility and elastic anisotropy at ambient
275 conditions and, more generally, in the low-*P* regime (Figure 4).

276 The same conclusion is valid for the synthetic hydroxycancrinite (Table 2), a cancrinite-
277 subgroup compound studied at high-pressure by Oh et al. (2011). It is worth noting that Oh et al.
278 (2011) also reported a subtle discontinuity in the *P*-*V* data between 1.9 and 2.5 GPa, although not
279 supported by structural data. The only other compound of the cancrinite group studied at high

pressure is the synthetic $Na_6Cs_2[Ga_6Ge_6O_{24}]\cdot Ge(OH)_6$ (Gatta and Lee 2008), which is the only one with a non-aluminosilicate framework studied at high pressure. To the different composition of the tetrahedral framework is likely ascribable the reported higher bulk compressibility (Table 2). The pronounced compression in the low-P regime of the $(Ga,Ge)O_4$ tetrahedra is, at least partially, responsible for the lower K_0 and for the elastic stiffening with increasing pressure (as suggested by the higher K'), if compared to the natural compounds all showing a "quasi-rigid" Si- or Al-tetrahedra.

All the cancrinite-group compounds studied at high pressure were found to be stable up to the highest pressures investigated (Table 2), with no hints of structural collapse or amorphization. In particular, davyne and balliranoite showed stability up to ~ 7 GPa without phase transitions or change of the compressional behavior (Lotti et al. 2014a, 2014b).

Thermal behavior of cancrinite-group minerals

Several studies have been devoted to the high-temperature behavior of cancrinite-group compounds. We will provide a brief overview of the behavior of natural samples, starting from the *in situ* single-crystal X-ray diffraction study of cancrinite *sensu stricto* performed by Gatta et al. (2014), who reported a very slow dehydration process at 748 K, which took 12 days to reach structural relaxation. Similarly, Sirbescu and Jenkins (1999) reported a thermogravimetric analysis of a synthetic sample of cancrinite (0.06 K/min average heating rate) which needed 10 days to fully dehydrate at 1058 K, with an intense weight-loss peak in the range 570-770 K. These results are in good agreement with the structure refinement performed by Gatta et al. (2014) at T above the dehydration temperature (*i.e.* 748 K), showing the presence of residual H_2O molecules within the *can* unit cages. It is worth noting the stability, or metastability, of the "quasi-anhydrous" cancrinite reported by Gatta et al. (2014) at least in the range 748-823 K, above which a broadening of the diffraction peaks suggested an impending decomposition or a severe deterioration of the long-range

order of the crystal. Interestingly, the dehydration was reported to be irreversible at the time-scale of the experiment, as confirmed by the diffraction data collected after the high-*T* ramp. The dehydration of a natural cancrinite was also reported by Isupova et al. (2010) by *in situ* single-crystal X-ray diffraction at 623 K, above which a dehydrated form was reported to be crystalline at least up to 823 K. An irreversible dehydration was also reported by Ballirano et al. (1995), on basis of an *ex situ* single-crystal X-ray diffraction experiment at room-*T* on a cancrinite sample previously heated up to 873 K.

These experimental observations may be coupled with the findings of natural partially anhydrous cancrinite crystals in volcanic alkaline rocks at the Eifel region, for which Zubkova et al. (2011) suggested the loss of H_2O in response to the roasting of the crystals during the effusive process. The high-*T* behavior of a natural cancrinite, showing superstructure reflections along the **c**-axis, was also studied by Hassan et al. (2006) by *in situ* synchrotron X-ray powder diffraction, reporting a discontinuity in the evolution of the unit-cell parameters at 777 K and a complete dehydration at 898 K. Loss of CO_2 was reported to occur at 1223 K by Hassan (1996a) on the basis of a TG-DTG analysis of a natural cancrinite, which was observed to melt at 1528 K. Sirbescu and Jenkins (1999) reported unchanged CO_3^{2-} signals from *ex situ* infra-red analysis of previously heated synthetic cancrinite up to 1153 K, where decomposition to a mixture of nepheline + haüyne was observed.

To the best of our knowledge, no high-temperature studies of the SO_4^{2-}-end member of the cancrinite subgroup (*i.e.* vishnevite) are available in the open literature. However, the high-*T* behavior of the K-rich pitiglianoite was performed by Bonaccorsi et al. (2007) by *in situ* single-crystal X-ray diffraction and FTIR spectroscopy. These authors reported a unit-cell expansion up to 499 K, followed by a dehydration process with unit-cell contraction in the range 499-676 K and a further expansion between 676 and 914 K. The dehydration was coupled with a partial and irreversible migration of the channel-K^+ cations into the *can* cages and cage-Na^+ into the channel

330 sites, which likely played a role in the minor re-adsorption of H_2O observed with decreasing
331 temperature. These data point out the significant influence of the extraframework constituents on
332 the (*P*,*T*)-induced transformations of cancrinite-group minerals. The presence of CO_2 molecules,
333 along with SO_4^{2-} anions, within the structural channels was confirmed by FTIR spectra, which
334 suggested, as reported by Bonaccorsi et al. (2007), a full loss of CO_2 at $T \geq 723$ K.

335 The major difference between the high-*T* behavior of the cancrinite- and davyne-subgroup
336 minerals can be found in the (nominally) anhydrous nature of the latter. Bonaccorsi et al. (1995)
337 reported the high-*T* study of both $P6_3$-davyne and $P6_3$-microsommite, by *in situ* single-crystal X-
338 ray diffraction, observing a similar thermal expansion with a clear discontinuity in the evolution of
339 the cell parameters and a decrease of the thermal expansivity along the **c**-axis (Table 2) at 473 (for
340 davyne) and 433 K (for microsommite). This discontinuity is due to the displacive phase transition
341 to the $P6_3/m$ space group, induced by the expansion of the *dzc* chains, *via* tetrahedral tilting, to the
342 geometric limit for which the inter-tetrahedral O3-O4-O3 angle is 180° (O3-O3-O3 in space group
343 $P6_3/m$, Figure 5). This symmetry-constraint prevents a further expansion of the *dzc* chains by
344 tetrahedral tilting and is responsible for the decrease of the thermal expansivity along the [0001]
345 direction.

346 Bonaccorsi et al. (1995) also reported the high-*T* behavior of a davyne sample with $P6_3/m$
347 symmetry at room conditions, for which insignificant thermal expansion along the **c**-axis was
348 observed even at the low-temperature regime (Table 2). The high-*T* behavior of microsommite was
349 later studied by Bonaccorsi et al. (2001), by *in situ* single-crystal X-ray diffraction and Monte Carlo
350 simulation, in order to define the order-disorder processes of the extraframework population. The
351 authors reported a full disorder (*i.e.* in response to a complete microsommite-to-davyne structure
352 transformation) at the critical temperature of 1023 K.

353 If the *T*-induced dehydration may act as a destabilizing factor affecting the cancrinite-
354 subgroup compounds, in the nominally anhydrous davyne-subgroup minerals a potential source of

355 thermal instability is represented by the *T*-induced phase transition to the $P6_3/m$ space group, which
356 hinders the deformation mechanisms able to accommodate the structural expansion along the **c**-axis
357 *via* tetrahedral tilting.

358 When not affected by dehydration processes, all minerals of the cancrinite group show
359 comparable bulk thermal expansivities (Hassan et al. 2006; Gatta et al. 2012a, 2013a, 2013b, 2014),
360 and the stacking direction of the 6-rings layers ([0001]-axis) is the most expandable one. Two
361 different anisotropic patterns can be defined for the minerals belonging to the two subgroups, more
362 pronounced for cancrinite-subgroup minerals (Table 2).

363

364 **Mechanisms of crystal structure deformation at non-ambient conditions**

365 - *Mechanisms of framework deformation*

366 The different coordination environment of the Na^+ cation, compared with that of Ca^{2+}
367 (Figure 2), leads to a framework contraction of cancrinite and vishnevite in the (0001) plane already
368 at room conditions. Moreover, beside the different ditrigonal character of the S6R⊥[0001] (Figure
369 1), a different configuration of the channel voids is also observed among the cancrinite-group
370 minerals. In cancrinite subgroup, the ~ 1:1 ratio of the symmetry-independent O1-$O1_{12R}$ and O3-
371 $O4_{12R}$ diameters (Figure 6) gives an almost circular shape of the section perpendicular to the **c** axis;
372 in davyne subgroup, a markedly hexagonal section occurs (Figure 1), with a smaller effective pore
373 width (*sensu* Baerlocher et al. 2007). In addition, the presence of $[Ca{\cdot}Cl]^+$ clusters in the cages
374 and/or SO_4^{2-} anions (with associated K^+ cations) in the channels leads to an expansion of the *dzc*
375 chains along [0001] already at room conditions. As a consequence, the *dzc* chains are more
376 expanded in vishnevite than cancrinite and in davyne than balliranoite.

The different extraframework population in cancrinite- and davyne-subgroup members is not only the source for the different framework configurations at ambient conditions, but also the cause of the different distortion mechanisms in response to temperature or pressure. In the following paragraphs, we provide a model of the structural evolution of cancrinite-group minerals at non-ambient conditions, on the basis of the high-*P* studies of Lotti (2014) and Lotti et al. (2012, 2014a, 2014b) and the low- and high-*T* studies of Bonaccorsi et al. (1995, 2007), Hassan et al. (2006), Isupova et al. (2010) and Gatta et al. (2012a, 2013a, 2013b, 2014).

The analysis of the *T*- and *P*-induced evolution of the Si-O-Al inter-tetrahedral angles shows that two distinct trends can be defined for the cancrinite- and davyne-subgroup minerals, respectively. In cancrinite subgroup, all the four symmetry-independent Si-O-Al angles vary with *T* or *P* (Figure 7, Tables 3 and 4 - deposited). In davyne subgroup, no significant variations of the Si-O2-Al angle are observed and the Si-O1-Al angle always shows the greatest change with *T* or *P* (Figure 7, Tables 3 and 4). These different trends are the basis for different deformation mechanisms in the two subgroups.

The framework deformation along [0001] is controlled by the tilting of the tetrahedra forming the *dzc* chains, around the O3 and O4 hinges (Figures 1 and 5), which correlates with the Si-O3-Al and Si-O4-Al inter-tetrahedral angles. The behavior of these angles with *P* and *T* does not show any significant difference between the two subgroups of minerals (Tables 3 and 4). The same deformation mechanism accommodates the strain along the **c**-axis: the expansion or compression of the *dzc* chains is well described by the change in the O3-O4-O3 angle (Figures 5 and 6; Tables 3 and 4). When the maximum expansion limit of 180° is reached, the displacive phase transition from the $P6_3$ to the $P6_3/m$ space group occurs (Bonaccorsi et al. 1995). Similarly, the reverse transition occurs when pressure is applied to a davyne sample showing $P6_3/m$ symmetry at room conditions (Lotti et al. 2014a).

The main differences between the two subgroups are in the mechanisms accommodating the strain within the (0001) plane, mainly governed by the tilting of the tetrahedra around the O1 and O2 hinges, correlated with the Si-O1-Al and Si-O2-Al inter-tetrahedral angles. In cancrinite and vishnevite, a strong variation in the ditrigonal shape of the S6R⊥[0001] occurs in response to *T* and *P*, and the bulk compression/expansion is accommodated by both the S4R's (along O3-O4) and by the channels (along O1-O1) (Figure 6; Tables 3 and 4). In contrast, balliranoite and davyne show less intense "ditrigonalization" of the cage bases, and the compression/expansion on the (0001) plane is mainly accommodated by the channel diameters (Figure 6; Tables 3 and 4). Overall, for all the studied minerals, the contribution of the channel voids to the bulk compressibility/expansivity was found to be significantly higher than that of the *can* cages (Lotti 2014).

- *Behavior of extraframework population at non-ambient conditions*

The high-*P* and low-*T* studies of cancrinite (Lotti et al. 2012; Gatta et al. 2012a) and vishnevite (Lotti 2014) showed, in response to pressure or low temperature, a compression of the first tetrahedral shell of the Na coordination environment into the cage (involving three O2 and the closer Ow sites) and an anisotropic expansion of the second shell (Tables 3 and 4). In other words, the distortion of the bipyramidal polyhedron is further enhanced in a "compressive" regime (*i.e.* high-*P* and low-*T*), leading to an increasingly tetrahedral form of the Na-coordination. In contrast, only minor changes occur for the Ca-O bonds in balliranoite and davyne at the same conditions (Tables 3 and 4; Gatta et al. 2013a, 2013b; Lotti et al. 2014a, 2014b). This markedly different behavior reflects the different evolution with *T* and *P* of the Si-O2-Al inter-tetrahedral angle between the two subgroups (Tables 3 and 4). In fact, the inhibited tetrahedral rotation around the O2 hinge (Figure 6) in davyne-subgroup minerals prevents the migration of this oxygen toward the Ca^{2+} cation and, as a consequence, a significant compression of the Ca-O2 bonds (Figure 2). Such a different behavior may be ascribed to the nature of the cage cations and their different coordination

426 configuration: the longer Ca-O bond lengths, if compared to Na-O ones, can explain the less
427 pronounced compression of the Ca-O2 bonds (than the Na-O2) in response to the applied *P* (or low-
428 *T*), leading to different framework deformation mechanisms than those observed in Na-members.

429 The analysis of the high-temperature behavior of cancrinite showed the same mechanisms
430 previously observed at low-*T* and high-*P*, but opposite in sign, at least at temperatures below the
431 start of dehydration (Table 4; Hassan et al. 2006; Isupova et al. 2010; Gatta et al. 2014). In response
432 to dehydration, an inversion in the *T*-induced trend of the Si-O2-Al inter-tetrahedral angle can be
433 observed from the H*T* studies of Isupova et al. (2010) and Gatta et al. (2014) (Table 4), likely to
434 minimize both the Na-O1 and Na-O2 bond lengths in order to counterbalance the loss of H_2O-
435 oxygen atoms. This mechanism concurs to the stability (or metastability) of the observed quasi-
436 anhydrous form of cancrinite in Nature.

437 The compression/expansion of the chemical bonds of the channel cations (M-$O_{framework}$, M =
438 Na, Ca, K) is strictly related to the distortion of the *dzc* chains along [0001]. In cancrinite,
439 balliranoite and davyne, no substantial change in the coordination of channel cations and anions
440 was observed at non-ambient conditions (Gatta et al. 2012a, 2013a, 2013b; Lotti et al. 2012, 2014a,
441 2014b). Therefore, for these minerals, the channel extraframework population apparently does not
442 have a significant effect on the behavior in response to the applied temperature or pressure. In
443 contrast, a re-arrangement of the channel population apparently occurs in vishnevite at $P \geq 3.43(4)$
444 GPa, coupled with a significant increase in compressibility (Lotti 2014). In vishnevite, a
445 displacement of the SO_4^{2-} tetrahedra around the 6_3-axis is followed by a significant migration of the
446 Na^+ cations towards the center of the channel. However, the marked increase in compressibility and
447 the unusual short K-O bonds suggest a metastable nature of the observed high-*P* configuration of
448 vishnevite (Lotti 2014). Nevertheless, these data show that even the channel constituents, and in
449 particular the cations bonding environment, might control the behavior and the stability of some
450 cancrinite-group species at non-ambient conditions. This is also substantiated by the high-*T*

451 behavior of pitiglianoite (Bonaccorsi et al. 2007), for which, at temperatures above the dehydration
452 process, an irreversible Na^+ / K^+ cationic exchange occur between channels and cages, with the
453 larger cations occupying the *can* units in the new high-*T* structural configuration.

454

455 **Implications**

456 The studies performed during the last decade on the behavior of cancrinite-group minerals at
457 non-ambient conditions, and here reviewed, allowed the experimental determination of the thermo-
458 elastic parameters of the most important end-members of this group (Table 2), whose
459 implementation in the thermodynamic datasets can be used for a better modelling of the complex
460 equilibria relating to natural rocks. Often, thermodynamic data (here isothermal compressibility or
461 isobaric thermal expansivity) are "estimated", when not known experimentally (*e.g.* Holland and
462 Powell 2011), giving rise to potentially crude results.

463 The crystal chemistry of cancrinite-group minerals is somehow unique: they are among the
464 few silicates which contain structurally incorporated H_2O and anionic groups as CO_3^{2-}, $C_2O_4^{2-}$,
465 SO_4^{2-} or Cl^-. Their open-frameworks allow also additional molecules to be entrapped into the
466 cavities, including CO_2. Della Ventura et al. (2007, 2008) reported, on the basis of infra-red
467 spectroscopic analyses, the presence of strong rim-to-core inhomogeneities in the volatile
468 composition of cancrinite-group minerals due to a CO_2/CO_3^{2-} substitution, pointing out the
469 sensitiveness of these compounds to the physical-chemical conditions of the crystallization
470 environments and suggesting their potential application as geochemical markers.

471 The high-*T* experiments made on the cancrinite group show that the anhydrous forms keep
472 their crystallinity even at 800-900 K, which is very high temperature for microporous structures.
473 High-*T* studies of cancrinite *sensu stricto* (*e.g.* Sirbescu and Jenkins 1999; Gatta et al. 2014) report
474 slow kinetics of dehydration under equilibrium conditions, if compared to other hydrous

475 microporous silicates, *e.g*. zeolites. Dehydration may likely occur under non-equilibrium conditions
476 in xenoliths involved in volcanic processes. Nevertheless, the stability, or mestability, of the
477 anhydrous (or partially-hydrous) form of cancrinite is reported in the literature (*e.g*. Ballirano et al.
478 1995; Hassan et al. 2006; Gatta et al. 2014) and is also confirmed by its occurrence in xenoliths
479 within alkaline basalts (Zubkova et al. 2011). The experiments on the *T*-induced dehydration of
480 cancrinite under equilibrium conditions (Sirbescu and Jenkins 1999; Gatta et al. 2014) suggests that
481 this process would occur at temperatures not lower than 650-750 K, at 0.0001 GPa. The combined
482 effect of *P* and *T* on the behavior of cancrinite-group minerals is basically unknown, and this, on
483 one hand, hinders a deep discussion on the petrological implications but, on the other hand, should
484 act as a stimulus for new experiments in this direction. The sub-solidus stabilities of some
485 cancrinite-group minerals were studied by Edgar (1964), who reported that cancrinite and
486 hydroxycancrinite were still stable at 1070 K and 0.13 GPa $P(H_2O)$, suggesting that, at a high-
487 enough carbonate fugacity, cancrinite should be stable at liquidus conditions.

488 The experimental findings of the host-guest interactions and of the structural deformation
489 mechanisms at high *T* and *P* show the relevant role played by the extraframework constituents, and
490 in particular of the cage population (Figure 2), on the behavior of cancrinite-group minerals at non-
491 ambient conditions. The *T*-induced mutual migration of K and Na between channels and cages in
492 pitiglianoite, at temperature above the dehydration process (Bonaccorsi et al. 2007), suggests the
493 potential high-thermal stability of the K-bearing members of the group, which should be further
494 investigated at high-*T* conditions. The modeling of the host-guest interactions at non-ambient
495 conditions provides a more robust background for the potential application of these compounds in
496 several technological fields: for example, by defining the high-*T* stability for a safe use of hydrous
497 cancrinite-subgroup compounds as solid storage-materials of alkaline wastes or for tailoring
498 preparation processes (Bao et al. 2005; Riley et al. 2012). Common precipitation of cancrinite-
499 group compounds were also reported from caustic nuclear waste solutions (*e.g.* Buck and

McNamara 2004; Rivera et al. 2011; Wang and Um 2013). The knowledge of the host-guest interactions in cancrinite-group materials with the structural cages occupied by large monovalent cations (*e.g.* K^+, Cs^+, Rb^+) is still poor, as well as their behavior under *T* or *P*. This configuration is shown only by tiptopite (which contains K^+) among the mineralogical species, but the synthesis of several Cs-cancrinites has successfully been reported (*e.g*. Colella and de' Gennaro 1989; Norby et al. 1991; Lee et al. 2000; Fechtelkord et al. 2001; Bieniok et al. 2005; Gatta and Lee 2008), whose thermal (and compressional) stability is still unknown. The confinement of Cs^+ (or Rb^+) cations inside the *can* units, with their small effective pore widths (*sensu* Baerlocher et al. 2007), suggests the potential application of cancrinite-group minerals as nuclear waste storage materials, as recently reported for other classes of microporous materials (*e.g.* Gatta et al. 2008b, 2009a, 2009b, 2012b; Sanchez-Valle et al. 2010). In this light, experiments on the thermo-elastic behavior, (*P*,*T*)-phase stability and chemical stability (by leaching processes) of Cs-cancrinites are necessary, for their potential utilization.

The behavior at non-ambient conditions of the cancrinite-group minerals shows, beside the potential destabilizing effects of temperature (*e.g*. dehydration in the cancrinite subgroup, $P6_3$-to-$P6_3/m$ phase transition in the compounds of davyne subgroup), a high-*P* stability (at room-*T*), which is quite surprising if we consider their microporous nature. The *P*-induced stability is the effect of a structural flexibility, which in turn is based mainly on tilting of rigid tetrahedra around O atoms that behave as hinges. In cancrinite-group minerals, the *P*-induced tilting of tetrahedra usually leads to continuous re-arrangements of the framework without any phase transition. As observed in other classes of open-framework silicates (*e.g.* zeolites), flexibility and microporosity do not necessarily imply high compressibility: the cancrinite-group minerals are less or similarly compressible than other rock-forming minerals (*e.g*. α-quartz, Angel et al. 1997; Na-rich feldspars, Benusa et al. 2005; tri- and di-octahedral micas, Zanazzi and Pavese 2002). In this light, the high-*P* experimental

524 findings on cancrinite-group minerals, here reviewed, corroborate the conclusion of Gatta (2008) on
525 zeolites, which can also be extended to this group of feldspathoids: "*porous does not mean soft*".

526

527

Acknowledgements

The authors thank Fernando Càmara (Univ. of Turin), Volker Kahlenberg (Univ. of Innsbruck), Marco Merlini and Nicola Rotiroti (Univ. of Milan) and Fabio Bellatreccia (Univ. of Roma Tre) for their significant contribution to the research project on the behavior of cancrinite-group minerals at non-ambient conditions. The Italian Ministry of Education, MIUR Project: "Futuro in Ricerca 2012 – ImPACT-RBFR12CLQD" is acknowledged. R.X. Fischer, M. Welch and M. Kunz are thanked for the revision of the manuscript.

References

Angel, R.J. (2000) Equations of state. In R.M. Hazen, and R.T. Downs, Eds., High-Temperature and High-Pressure Crystal Chemistry, 41, p. 35-60. Reviews in Mineralogy and Geochemistry, Mineralogical Society of America and Geochemical Society, Chantilly, Virginia.

Angel, R.J., Allan, D.R., Miletich, R., and Finger, L.W. (1997) The use of quartz as an internal pressure standard in high-pressure crystallography. Journal of Applied Crystallography, 30, 461-466.

Angel, R.J., Alvaro, M., and Gonzalez-Platas, J. (2014) EosFit7c and a Fortran module (library) for equation of state calculations. Zeitschrift für Kristallographie , 229, 405-419.

Baerlocher, C., McCusker, L.B., and Olson, D.H. (2007) Atlas of Zeolite Framework Types, 6th ed., 398 p. Elsevier, Amsterdam.

Ballirano, P., Maras, A., Caminiti, R., and Sadun, C. (1995) Carbonate-cancrinite: in situ real-time thermal processes studied by means of energy-dispersive X-ray powder-diffractometry. Powder Diffraction , 10, 173-177.

Bao, Y., Grutzek, M.W., and Jantzen, C.M. (2005) Preparation and properties of hydroceramic waste forms made with simulated Hanford low-acitivity waste. Journal of American Ceramic Society , 88, 3287-3302.

Bell, K., Dunworth, E.A., Bulakh, A.G., and Ivanikov, V.V. (1996) Alkaline rocks of the Turiy pensisula, Russia, including type-locality turjaite and turjite: a review. Canadian Mineralogist , 34, 265-280.

Benusa, M.T., Angel, R.J., and Ross, N.L.(2005) Compression of Albite, $NaAlSi_3O_8$. American Mineralogist, 90, 1115-1120.

Berman, R.G. (1988) Internally-consistent thermodynamic data for minerals in the system Na_2O-K_2O-CaO-MgO-FeO-Fe_2O_3-Al_2O_3-SiO_2-TiO_2-H_2O-CO_2. Journal of Petrology, 29, 445-522.

Bieniok, A., Brendel, U., Paulus, E.F., and Amthauer, G. (2005) Microporous cobalto- and zinco-phosphates with the framework-type of cancrinite. European Journal of Mineralogy, 17, 813-818.

Birch, F. (1947) Finite elastic strain of cubic crystals. Physical Review, 71, 809-824.

Bonaccorsi, E., and Merlino, S. (2005) Modular microporous minerals: cancrinite-davyne group and C-S-H phases. In G. Ferraris, and S. Merlino, Eds., Micro- and Mesoporous Mineral Phases, 57, p. 241-290. Reviewsin Mineralogy and Geochemistry, Mineralogical Society of America and Geochemical Society, Chantilly, Virginia.

Bonaccorsi, E., Merlino, S., and Pasero, M. (1990). Davyne: its structural relationship with cancrinite and vishnevite. Neues Jahrbuch für Mineralogie-Monatshefte, 97-112.

Bonaccorsi, E., Merlino, S., Orlandi, P., Pasero, M., and Vezzalini, G. (1994) Quadridavyne $[(Na,K)_6Cl_2][Ca_2Cl_2][Si_6Al_6O_{24}]$, a new feldspathoid mineral from Vesuvius area. European Journal of Mineralogy, 6, 481-487.

573 Bonaccorsi, E., Comodi, P., and Merlino, S. (1995) Thermal behaviour of davyne-group
574 minerals. Physics and Chemistry of Minerals, 22, 367-374.

575 Bonaccorsi, E., Merlino, S., Pasero, M., and Macedonio, G. (2001) Microsommite: crystal
576 chemistry, phase transitions, Ising model and Monte Carlo simulations. Physics and Chemistry of
577 Minerals, 28, 509-522.

578 Bonaccorsi, E., Della Ventura, G., Bellatreccia, F., and Merlino, S. (2007) The thermal
579 behaviour and dehydration of pitiglianoite, a mineral of the cancrinite-group. Microporous and
580 Mesoporous Materials, 99, 225-235.

581 Brigatti, M.F., and Guggenheim, S. (2002) Mica crystal chemistry and the influence of
582 pressure, temperature and solid solution on atomistic models. In A. Mottana, F.P. Sassi, J.B.
583 Thompson, and S. Guggenheim, Micas: Crystal Chemistry and Metamorphic Petrology, 46, p. 1-98.
584 Reviews in Mineralogy and Geochemistry, Mineralogical Society of America and Geochemical
585 Society, Chantilly, Virginia.

586 Buck, E.C., and McNamara, B.K. (2004) Precipitation of nitrate-cancrinite in Hanford tank-
587 sludge. Environmental Science and Technology, 38, 4432-4438.

588 Chukanov, N.V., Pekov, I.V., Olysych, L.V., Massa, W., Yakubovich, O.V., Zadov, A.E.,
589 Rastsvetaeva, R.K., and Vigasina, M.F. (2010a) Kyanoxalite, a new cancrinite-group mineral
590 species with extraframework oxalate anion from the Lovozero alkaline pluton, Kola peninsula.
591 Geology of Ore Deposits, 52, 778-790.

592 Chukanov, N.V., Zubkova, N.V., Pekov, I.V., Olysych, L.V., Bonaccorsi, E., and
593 Pushcharovsky, D.Y. (2010b). Balliranoite, $(Na,K)_6Ca_2(Si_6Al_6O_{24})Cl_2(CO_3)$, a new cancrinite-group
594 mineral from Monte Somma - Vesuvio volcanic complex, Italy. European Journal of Mineralogy,
595 22, 113-119.

596 Colella, C., and de' Gennaro, M. (1989) Cancrinite crystallization from alkaline
597 aluminosilicate systems containing large and small cations. In M.L. Occelli, and H.E. Robson,
598 Zeolite synthesis, 398, p. 196-208. ACS Symposium Series, American Chemical Society.

599 Deer, W.A., Howie, R.A., Wise, W.S., and Zussman, J. (2004) Rock-forming minerals.
600 Framework silicates: silica minerals, feldspathoids and the zeolites, Vol. 4B, The Geological
601 Society, London.

602 Della Ventura, G., Bellatreccia, F., and Bonaccorsi, E. (2005) CO_2 in minerals of the
603 cancrinite-sodalite group: pitiglianoite. European Journal of Mineralogy, 17, 847-851.

604 Della Ventura, G., Bellatreccia, F., Parodi, G.C., Càmara, F., and Piccinini, M. (2007)
605 Single-crystal FTIR and X-ray study of vishnevite, ideally $[Na_6(SO_4)][Na_2(H_2O)_2](Si_6Al_6O_{24})$.
606 American Mineralogist , 92, 713-721.

607 Della Ventura, G., Bellatreccia, F., and Piccinini, M. (2008) Channel CO_2 in feldspathoids:
608 new data and new perspectives. Rendiconti Lincei-Scienze Fisiche e Naturali, 19, 141-159.

609 Edgar, A.D. (1964) Studies on cancrinites: II – Stability fields and cell dimensions of
610 potassium and potassium-rich cancrinites. Canadian Mineralogist, 8, 53-67.

611 Edgar, A.D. (1984) Chemistry, occurrence and paragenesis of feldspathoids: A review. In
612 W.L. Brown, Ed., Feldspars and Feldspathoids: Structures, Properties and Occurrences, 137, 501-
613 532. NATO ASI Series, Series C: Mathematical and Physical Sciences.

614 Erd, R.C., and Czamanske, G.K. (1983) Orickite and coyoteite, two new sulfides minerals
615 from Coyote Peak, Humboldt County, California. American Mineralogist, 68, 245-254.

616 Fall, A., Bodnar, R.J., Szabò, C., and Pàl-Molnàr, E. (2007) Fluid evolution in the nepheline
617 syenite of the Ditrau alkaline massif, Tansylvania, Romania. Lithos , 91, 331-345.

618 Fechtelkord, M., Posnatzki, B., Buhl, J.-C., Fyfe, C.A., Groat, L.A., and Raudsepp, M.
619 (2001) Characterization of synthetic Cs-Li cancrinite grown in a butanediol-water system; an NMR
620 spectroscopic and Rietveld refinement study. American Mineralogist, 86, 881-888.

621 Foit, F.F., Peacor, D.R., and Heinrich, E.W. (1973) Cancrinite with a new superstructure
622 from Bancroft, Ontario. Canadian Mineralogist, 11, 940-951.

623 Fulignati, P., Panichi, C., Sbrana, A., Caliro, S., Gioncada, A., and Del Moro, A. (2005)
624 Skarn formation at the walls of the 79 AD magma chamber of Vesuvius (Italy): mineralogical and
625 isotopic constraints. Neues Jahrbuch für Mineralogie-Abhandlungen, 181/1, 53-66.

626 Gatta, G.D. (2008) Does porous mean soft? On the elastic behaviour and structural evolution
627 of zeolites under pressure. Zeitschrift für Kristallographie, 223, 160-170.

628 Gatta G.D. (2010) Extreme deformation mechanisms in open-framework silicates at high-
629 pressure: Evidence of anomalous inter-tetrahedral angles. Microporous and Mesoporous Materials,
630 128, 78–84.

631 Gatta, G.D. and Angel, R.J. (2007) Elastic behavior and pressure-induced structural
632 evolution of nepheline: implications for the nature of the modulated superstructure. American
633 Mineralogist, 92, 1446-1455.

634 Gatta, G.D., and Lee, Y. (2008) Pressure-induced structural evolution and elastic behaviour
635 of $Na_6Cs_2Ga_6Ge_6O_{24}{\cdot}Ge(OH)_6$ variant of cancrinite: A synchrotron powder diffraction study.
636 Microporous and Mesoporous Materials, 116, 51-58.

637 Gatta, G.D. and Lee, Y. (2014) Zeolites at high pressure: A review. Mineralogical
638 Magazine, 78, 267-291.

639 Gatta, G.D., Nestola, F., and Boffa Ballaran, T. (2006) Elastic behavior, phase transition and
640 pressure induced structural evolution of analcime. American Mineralogist, 91, 568-578.

641 Gatta, G.D., Rotiroti, N., Boffa Ballaran, T., and Pavese, A. (2008a) Leucite at high-
642 pressure: elastic behaviour, phase stability and petrological implications. American Mineralogist,
643 93, 1588-1596.

644 Gatta, G.D., Rotiroti, N., Zanazzi, P.F., Rieder, M., Drabek, M., Weiss, Z., and Klaska, R.
645 (2008b) Synthesis and crystal structure of the feldspathoid $CsAlSiO_4$: an open-framework silicate
646 and potential nuclear waste disposal phase. American Mineralogist, 93, 988-995.

647 Gatta, G.D., Rinaldi, R., McIntyre, G.J., Nénert, G., Bellatreccia, F., Guastoni, A., and Della
648 Ventura, G. (2009a) On the crystal structure and crystal chemistry of pollucite,
649 $(Cs,Na)_{16}Al_{16}Si_{32}O_{96}{\cdot}nH_2O$: a natural microporous material of interest in nuclear technology.
650 American Mineralogist, 94, 1560-1568.

651 Gatta, G.D., Rotiroti, N., Boffa Ballaran, T., Sanchez-Valle, C., and Pavese, A. (2009b)
652 Elastic behavior and phase-stability of pollucite, a potential host for nuclear waste. American
653 Mineralogist, 94, 1137-1143.

654 Gatta, G.D., Angel, R.J., and Carpenter, M.A. (2010) Low-temperature behaviour of natural
655 kalsilite with *P*31*c* symmetry: an in-situ single-crystal X-ray diffraction study. American
656 Mineralogist, 95, 1027-1034.

657 Gatta, G.D., Angel, R.J., Zhao, J., Alvaro, M., Rotiroti, N., and Carpenter, M.A. (2011)
658 Phase stability, elastic behavior, and pressure-induced structural evolution of kalsilite: A ceramic
659 material and high-*T*/high-*P* mineral. American Mineralogist, 96, 1363–1372.

660 Gatta, G.D., Lotti, P., Kahlenberg, V., and Haefeker, U. (2012a) The low-temperature
661 behaviour of cancrinite: an in situ single-crystal X-ray diffraction study. Mineralogical Magazine,
662 76, 933-948.

663 Gatta, G.D., Merlini, M., Lotti, P., Lausi, A., and Rieder, M. (2012b) Phase stability and
664 thermo-elastic behavior of CsAlSiO4 (ABW): A potential nuclear waste disposal material.
665 Microporous and Mesoporous Materials, 163, 147–152.

666 Gatta, G.D., Lotti, P., Nénert, G., and Kahlenberg, V. (2013a) On the crystal structure and
667 low-temperature behaviour of davyne: A single-crystal X-ray and neutron diffraction study.
668 Microporous and Mesoporous Materials, 185, 137-148.

669 Gatta, G.D., Lotti, P., and Kahlenberg, V. (2013b) The low-temperature behavior of
670 balliranoite (CAN topology): An in situ single-crystal X-ray diffraction study. Microporous and
671 Mesoporous Materials, 174, 44-53.

672 Gatta, G.D., Comboni, D., Alvaro, M., Lotti, P., Càmara, F., and Domeneghetti, M.C.
673 (2014) Thermoelastic behavior and dehydration process of cancrinite. Physics and Chemestry of
674 Minerals, 41, 373-386.

675 Gies, H., Kirchner, R., van Koningsveld, H., and Treacey, M.M.J. (1999) Faulted Zeolite
676 framework structures. Proc. 12th International Zeolite Conference, Baltimore, Maryland, U.S.A.,
677 July 5-11, 1998; eds. M.M.J. Treacey, B.K. Marcus, M.E. Bisher, J.B. Higgins, Materials Research
678 Society, Warrendale, Pennsylvania, 2999-3029.

679 Grossman, L. (1980) Refractory inclusions in the Allende meteorite. Annual Review of
680 Earth and Planetary Sciences, 8, 559-608.

681 Grundy, H.D., and Hassan, I. (1982) The crystal structure of a carbonate-rich cancrinite.
682 Canadian Mineralogist, 20, 239-251.

683 Harlow, G.E., and Bender, W. (2013) A study of ruby (corundum) composition from the
684 Mogok Belt, Myanmar: searching for chemical fingerprints. American Mineralogist, 98, 1120-1132.

685 Hassan, I. (1996a) The thermal behavior of cancrinite. Canadian Mineralogist, 34, 893-900.

686 Hassan, I. (1996b) Thermal expansion of cancrinite. Mineralogical Magazine, 60, 949-956.

687 Hassan, I., and Grundy, H.D. (1984) The character of cancrinite-vishnevite solid solution
688 series. Canadian Mineralogist, 22, 333-340.

689 Hassan, I., and Grundy, H.D. (1990) Structure of davyne and implications for stacking
690 faults. Canadian Mineralogist, 28, 341-349.

691 Hassan, I., and Buseck, P.R. (1992) The origin of the superstructure and modulations in
692 cancrinite. Canadian Mineralogist, 30, 49-59.

693 Hassan, I., Antao, S.M., and Parise, J.B. (2006) Cancrinite: Crystal structure, phase
694 transitions and dehydration behavior with temperature. American Mineralogist, 91, 1117-1124.

695 Holland, T.J.B. and Powell, R. (2011) An improved and extended internally consistent
696 thermodynamic dataset for phases of petrological interest, involving a new equation of state for
697 solids. Journal of Metamorphic Geology, 29, 333–383.

698 Isupova, D., Ida, A., Kihara, K., Morishita, T., and Bulka, G. (2010) Asymmetric thermal
699 vibrations of atoms and pyroelectricity in cancrinite. Journal of Mineralogical and Petrological
700 Sciences, 105, 29-41.

701 Jarchow, O. (1965) Atomanordnung und strukturverfeinerung von cancrinit. Zeitschrift für
702 Kristallographie, 122, 407-422.

703 Lee, Y., Parise, J.B., Tripathi, A., Kim, S.J., and Vogt, T. (2000) Synthesis and crystal
704 structures of gallium and germanium variants of cancrinite. Microporous and Mesoporous
705 Materials, 39, 445-455.

706 Löns, J. and Schulz, H. (1967) Strukturverfeinerung von Sodalith, $Na_8Si_6A1_6O_{24}C1_2$. Acta
707 Crystallographica, 23, 434-436.

Lotti, P. (2014) Cancrinite-group minerals at non-ambient conditions: a model of the elastic behavior and structure evolution. Ph.D. thesis, University of Milan (Italy), p. 306.

Lotti, P., Gatta, G.D., Rotiroti, N., and Càmara, F. (2012) High-pressure study of a natural cancrinite. American Mineralogist, 97, 872-882.

Lotti, P., Gatta, G.D., Merlini, M., and Hanfland, M. (2014a) High-pressure behavior of davyne [CAN-topology]: An in situ single-crystal synchrotron diffraction study. Microporous and Mesoporous Materials, 198, 203-214.

Lotti, P., Gatta, G.D., Rotiroti, N., Càmara, F., and Harlow, G.E. (2014b) The high-pressure behavior of balliranoite: a cancrinite-group mineral. Zeitschrift für Kristallographie , 229, 63-76.

Merlino, S. (1984) Feldspathoids: Their average and real structures. In W.L. Brown, Ed., Feldspars and Feldspathoids: Structures, Properties and Occurrences, 137, p. 435-470. NATO ASI Series, Series C: Mathematical and Physical Sciences.

Merlino, S., Mellini, M., Bonaccorsi, E., Pasero, M., Leoni, L., and Orlandi, P. (1991) Pitiglianoite, a new feldspathoid from southern Tuscany, Italy: chemical composition and crystal structure. American Mineralogist, 76, 2003-2008.

Norby, P., Krogh Andersen, I.G., Krogh Andersen, E., Colella, C., and de' Gennaro, M. (1991) Synthesis and structure of lithium cesium and lithium thallium cancrinites. Zeolites, 11, 248-253.

Ogorodova, L.P., Mel'chakova, L.V., Vigasina, M.F., Olysych, L.V., and Pekov, I.V. (2009) Cancrinite and cancrisilite in the Khibina-Lovozero alkaline complex: thermochemical and thermal data. Geochemistry International, 47, 260-267.

729 Oh, J.E., Clark, S.M., and Monteiro, P.J.M. (2011) Determination of the bulk modulus of
730 hydroxycancrinite, a possible zeolitic precursor in geopolymers, by high-pressure synchrotron X-
731 ray diffraction. Cement and Concrete Composites, 33, 1014-1019.

732 Olysych, L.V., Vigasina, M.F., Mel'chakova, L.V., Ogorodova, L.P., Pekov, I.V., and
733 Chukanov, N.V. (2011) Thermal evolution and thermochemistry of the cancrinite-group carbonate-
734 oxalate mineral. Geochemistry International, 49, 731-737.

735 Pauling, L. (1930) The structure of some sodium and calcium aluminosilicates. Proceedings
736 of the National Academyof Sciences, 16, 453-459.

737 Peacor, D.R., Rouse, R.C., and Ahn, J.-H. (1987) Crystal structure of tiptopite, a framework
738 berillophosphate isotypic with basic cancrinite. American Mineralogist, 72, 816-820.

739 Pekov, I.V., Olysych, L.V., Chukanov, N.V., Zubkova, N.V., and Pushcharovsky, D.Y.
740 (2011a). Crystal chemistry of cancrinite-group minerals with an AB type framework: a review and
741 new data. I. Chemical and structural variations. Canadian Mineralogist, 49, 1129-1150.

742 Pekov, I.V., Olysych, L.V., Zubkova, N.V., Chukanov, N.V., Van, K.V., and
743 Pushcharovsky, D.Y. (2011b) Depmeierite $Na_8[Al_6Si_6O_{24}](PO_4,CO_3)_{1-x}*3H_2O$ ($x<0.5$): a new
744 cancrinite-group mineral species from the Lovozero alkaline pluton of the Kola peninsula. Geology
745 of Ore Deposits, 53, 604-613.

746 Rastsvetaeva, R.K., Pekov, I.V., Chukanov, N.V., Rozenberg, K.A., and Olysych, L.V.
747 (2007) Crystal Structures of Low-Symmetry Cancrinite and Cancrisilite Varieties. Crystallography
748 Report, 52, 811-818.

749 Riley, B.J., Crum, J.V., Matyas, J., McCloy, J.S., and Lepry, W.C. (2012) Solution-derived,
750 chloride-containing minerals as a waste form for alkali chlorides. Journal of American Ceramic
751 Society, 95, 3115-3123.

Rivera, N.A., Choi, S., Strepka, C., Mueller, K.T., Chorover, J., and O'Day, P.A. (2011) Cesium and strontium incorporation into zeolite-type phases during homogeneous nucleation from caustic solution. American Mineralogist, 96, 1809-1820.

Rouquerol, J., Avnir, D., Fairbridge, C.W., Everett, D.H., Haynes J.M., Pernicone, N., Ramsay, J.D.F., Sing, K.S.W., and Unger K.K. (1994) Recommendations for the characterization of porous solids (Technical Report). Pure and Applied Chemistry, 66, 1739-1758.

Sanchez-Valle, V., Chio, C-H., and Gatta, G.D. (2010) Single-crystal elastic properties of (Cs,Na)$AlSi_2O_6$•H_2O pollucite: with potential use for long-term storage of Cs radioisotopes. Journal of Applied Physics, 108, 093509 (1-7).

Sapozhnikov, A.N. (2010) Crystal chemical features of davyne from Tultui lazurite deposit (Baikal region). Journal of Structural Chemistry, 51, 507-513.

Sindern, S., and Kramm, U. (2000) Volume characteristics and element transfer of fenite aureoles: a case-study from the Iivaara alkaline complex, Finland. Lithos, 51, 75-93.

Sirbescu, M., and Jenkins, D.M. (1999) Experiments on the stability of cancrinite in the system Na_2O-CaO-Al_2O_3-SiO_2-CO_2-H_2O. American Mineralogist, 84, 1850-1860.

Smith, J.V. (2000) Tetrahedral frameworks of zeolites, clathrates and related materials. Landolt-Börnstein - Group IV Physical Chemistry, 14A, 251-266.

Wang, G., and Um, W. (2013) Facilitated strontium transport by remobilization of strontium-containing secondary precipitates in Hanford site subsurface. Journal of Hazardous Materials, 248-249, 364-370.

Zanazzi, P.F., and Pavese, A. (2002) Behavior of Micas at High-Pressure and High-Temperature. In A. Mottana, F.P. Sassi, J.B. Thompson, and S. Guggenheim, Eds., Micas: Crystal

774 Chemistry and Metamorphic Petrology, 46, p. 99-116. Reviews in Mineralogy and Geochemistry,
775 Mineralogical Society of America and Geochemical Society, Chantilly, Virginia.

776 Zubkova, N.V., Chukanov, N.V., Pekov, I.V., and Pushcharovsky, D.Y. (2011) Low-
777 hydrous cancrinite: atomic structure and indicative importance. Doklady Earth Sciences, 439, 998-
778 1001.

779

780

781 **Table 1.** Cancrinite-group minerals.

782

	Chemical formula, *Z*	Unit-cell constants (a, c; Å)	Space group	Ref.
Cancrinite subgroup:				
cancrinite	$[(Na,Ca)_6(CO_3)_{1.4\text{-}1.7}][Na_2(H_2O)_2][Si_6Al_6O_{24}]$, 1	12.615, 5.127	$P6_3$	*a*
vishnevite	$[(Na,K)_6(SO_4)][Na_2(H_2O)_2][Si_6Al_6O_{24}]$, 1	12.685, 5.179	$P6_3$	*a, b*
hydroxycancrinite	$[Na_6(OH)_2][Na_2(H_2O)_2][Si_6Al_6O_{24}]$, 1	12.740, 5.182	$P3$	*a*
cancrisilite	$Na_7Al_5Si_7O_{24}(CO_3)\cdot 3H_2O$, 1	12.575, 5.105	$P6_3mc$	*a*
pitiglianoite	$[(Na_4K_2)(SO_4)][Na_2(H_2O)_2][Si_6Al_6O_{24}]$, 3	22.121, 5.221	$P6_3$	*a*
kyanoxalite	$[Na_5(C_2O_4)_{0.5\text{-}1}(H_2O)_{2\text{-}3}][NaH_2O]_2[Si_{6\text{-}7}Al_{5\text{-}6}O_{24}]$, 1	12.74, 5.21	$P6_3$	*c*
depmeierite	$[Na_6(PO_4)_{0.67}H_2O][NaH_2O]_2[Si_6Al_6O_{24}]$, 1	12.73, 5.18	$P6_3$	*c*
Davyne subgroup:				
davyne	$[(Na,K)_6(SO_4,Cl)][Ca_2Cl_2][Si_6Al_6O_{24}]$, 1	12.705, 5.368	$P6_3/m$ or $P6_3$	*a, d*
balliranoite	$[(Na,Ca)_6(CO_3)_{1.4\text{-}1.7}][CaCl]_2[Al_6Si_6O_{24}]$, 1	12.695, 5.325	$P6_3$	*a, e*
microsommite	$[Na_4K_2(SO_4)][Ca_2Cl_2][Si_6Al_6O_{24}]$, 3	22.142, 5.345	$P6_3$	*a*
quadridavyne	$[(Na,K)_6Cl_2][Ca_2Cl_2][Si_6Al_6O_{24}]$, 4	25.771, 5.371	$P6_3/m$	*a*
tiptopite	$[(Li_{2.9}Na_{1.7}Ca_{0.7})(OH)_2(H_2O)_{1.3}][K_2][Be_6P_6O_{24}]$; 1	11.655, 4.692	$P6_3$	*f*

Note: Chemical formulae based on 12 tetrahedral cations. References - *a*: Bonaccorsi and Merlino (2005); *b:* Della Ventura et al. (2007); *c*: Pekov et al. (2011a); *d*: Lotti et al. (2014a); *e*: Lotti et al.(2014b); *f*: Peacor et al. (1987).

783

784

785

786

787

788

789

790

791

792

793

794

795

796

797 **Table 2.** Thermo-elastic parameters of cancrinite-group minerals.

		***P*-range (GPa)**	**β_{V0} (GPa^{-1})**	**K_{V0} (GPa)**	**K_V'**	***T*-range (K)**	**$\alpha_{V(293K)}$ (10^{-5} K^{-1})**
Cancrinite	*a*	0.0001-4.62	0.022(1)	45(2)	6(1)		
	a	5.00-6.63	0.025(1)	40(2)	4		
	b					298-769	4.2(4)
	c					100-293	3.8(7)
	d					303-748	4.88(8)
	d					748-823	3.1(6)
Vishnevite	*e*	0.20-2.47	0.020(2)	49(4)	5.4(33)		
	e	3.83-7.40	0.033(3)	30(3)	2.6(5)		
Balliranoite	*f*	0.0001-6.77	0.021(1)	48(3)	4.0(10)		
	g					108-293	4.6(4)
Davyne ($P6_3$)	*h*	0.38-7.18	0.0215(5)	46.5(11)	3.7(3)		
	i					110-293	4.2(4)
	j					293-449	5.4(6) *
Davyne ($P6_3/m$)	*j*					503-948	3.0(1) *
	j					293-829	2.7(2) *
Microsommite ($P6_3$)	*j*					293-423	5.5(4) *
Microsommite ($P6_3/m$)	*j*					503-947	1.9(2) *
Hydroxycancrinite#	*k*	0.0001-6.1	0.0213(4)	46.9(9)	4.0(4)		
$Na_6Cs_2[Ga_6Ge_6O_{24}]\cdot Ge(OH)_6$#	*l*	0.0001-5.01	0.029(2)	35(2)	11(1)		

		***P*-range (GPa)**	**β_{a0} (GPa^{-1})**	**K_{a0} (GPa)**	**K_a'**	***T*-range (K)**	**$\alpha_{a(293K)}$ (10^{-5} K^{-1})**
Cancrinite	*a*	0.0001-4.62	0.0064(7)	52(6)	11(4)		
	a	5.00-6.63	0.0057(4)	58(4)	4		
	b					298-769	0.90(8)
	c					100-293	0.7(2)
	d					303-748	1.16(3)
	d					748-823	0.6(3)
Vishnevite	*e*	0.20-2.47	0.0060(4)	56(4)	7.3(32)		
	e	3.83-7.40	0.0083(6)	40(3)	1.8(4)		
Balliranoite	*f*	0.0001-6.77	0.0062(5)	54(4)	4.6(14)		
	g					108-293	1.4(2)
Davyne ($P6_3$)	*h*	0.38-7.18	0.0066(1)	50.3(9)	4.0(3)		
	i					110-293	1.4(1)
	j					293-449	1.69(8) *
Davyne ($P6_3/m$)	*j*					503-948	1.32(6) *
	j					293-829	1.34(7)
Microsommite ($P6_3$)	*j*					293-423	1.6(1) *
Microsommite ($P6_3/m$)	*j*					503-947	0.86(4) *
Hydroxycancrinite#	*k*	0.0001-6.1	0.0062(6)*	54(5)*	4*		
$Na_6Cs_2[Ga_6Ge_6O_{24}]\cdot Ge(OH)_6$#	*l*	0.0001-5.01	0.0083(4)	40(2)	11(1)		

		***P*-range (GPa)**	**β_{c0} (GPa^{-1})**	**K_{c0} (GPa)**	**K_c'**	**K_{a0}/K_{c0}**	***T*-range (K)**	**$\alpha_{c(293K)}$ (10^{-5} K^{-1})**	**α_{c0}/α_{a0}**
Cancrinite	*a*	0.0001-4.62	0.0098(6)	34(2)	2.8(8)	1.53			
	a	5.00-6.63	0.016(1)	20.6(14)	4	2.82			
	b						298-769	2.3(2)	2.55
	c						100-293	2.1(3)	3.00
	d						303-748	2.58(8)	2.22
	d						748-823	1.9(5)	3.17
Vishnevite	*e*	0.20-2.47	0.0090(5)	37(2)	5.0(20)	1.51			
	e	3.83-7.40	0.021(4)	16(3)	3.6(5)	2.50			
Balliranoite	*f*	0.0001-6.77	0.0083(4)	40(2)	3.3(6)	1.35			
	g						108-293	1.7(2)	1.21
Davyne ($P6_3$)	*h*	0.38-7.18	0.0083(1)	40.3(7)	3.2(2)	1.25			
	i						110-293	1.6(1)	1.14
	j						293-449	1.6(4)	0.95
Davyne ($P6_3/m$)	*j*						503-948	0.3(1)	0.23
	j						293-829	0.11(3) *	0.08
Microsommite ($P6_3$)	*j*						293-423	1.6(4)	1.00
Microsommite ($P6_3/m$)	*j*						503-947	0.2(1)	0.23
Hydroxycancrinite#	*k*	0.0001-6.1	0.0101(9) *	33(3) *	4*	1.64			
$Na_6Cs_2[Ga_6Ge_6O_{24}]\cdot Ge(OH)_6$#	*l*	0.0001-5.01	0.0108(3)	31(1)	7.4(8)	1.29			

Note: β_{V0} is the isothermal compressibility coefficient, K_{V0} and K_V' are the isothermal bulk modulus and its *P*-derivative, respectively, and $\alpha_{V(293K)}$ is the thermal expansion coefficient of the unit-cell volume; β_{j0}, K_{j0}, K_j', and $\alpha_{j(293K)}$ are the co-respective axial coefficients (with $j = a$, c);

References - *a*: Lotti et al. (2012); *b*: Hassan et al. (2006); *c*: Gatta et al. (2012a); *d*: Gatta et al. (2014); *e*: Lotti (2014); *f*: Lotti et al. (2014b); *g*: Gatta et al. (2013b); *h*: Lotti et al. (2014a); *i*: Gatta et al. (2013a); *j*: Bonaccorsi et al. (1995); *k*: Oh et al. (2010); *l*: Gatta and Lee (2008); * Calculated from published data; # Synthetic compounds.

798 **Table 3 (deposited).** Relevant inter-tetrahedral angles (°), voids diameters (Å), bond distances (Å) and the ditrigonal rotation angle (°) at different
799 pressures of cancrinite-group minerals.

800

P (GPa)	Si-O1-Al	Si-O2-Al	Si-O3-Al	Si-O4-Al	O3-O4-O3	$\alpha_{S6R\perp[0001]}$	$O3\text{-}O4_{S4R}$	$O1\text{-}O1_{12R}$	$O3\text{-}O4_{12R}$	(Na,Ca)-O1	(Na,Ca)-O2
					Cancrinite (Lotti et al. 2012)						
0.0001	147.5(7)	151.8(6)	131.4(6)	132.5(5)	142.9(4)	8.8(2)	4.15(1)	9.16(1)	8.48(1)	2.888(8)	2.441(7)
0.76(2)	145.4(7)	149.0(5)	131.3(6)	132.6(5)	141.1(4)	9.6(2)	4.08(1)	9.12(1)	8.51(2)	2.883(8)	2.397(6)
0.99(2)	145.9(7)	149.5(5)	132.2(5)	131.5(5)	143.1(3)	9.5(2)	4.13(1)	9.08(1)	8.41(1)	2.879(8)	2.403(6)
1.39(2)	143.9(6)	148.3(5)	131.3(4)	129.9(5)	140.3(3)	10.0(2)	4.09(1)	9.04(1)	8.432(9)	2.886(7)	2.380(6)
2.33(2)	143.6(6)	148.5(4)	130.4(4)	129.4(4)	140.1(3)	9.8(2)	4.07(1)	9.00(1)	8.388(8)	2.867(7)	2.374(6)
3.59(2)	141.4(7)	144.2(5)	128.9(5)	128.6(5)	136.5(3)	11.6(2)	3.99(1)	8.88(1)	8.405(8)	2.894(7)	2.312(6)
4.30(3)	140.7(6)	143.3(5)	128.6(5)	127.8(5)	135.7(3)	12.2(2)	3.97(1)	8.81(1)	8.380(8)	2.902(7)	2.286(7)
5.00(2)	139.6(6)	143.6(5)	127.7(4)	127.2(4)	135.1(3)	11.6(2)	3.98(1)	8.837(9)	8.351(8)	2.874(7)	2.291(6)
5.73(3)	137.6(7)	140.9(5)	126.0(5)	126.5(5)	133.1(4)	13.2(2)	3.91(1)	8.68(1)	8.377(9)	2.931(8)	2.262(7)
6.16(2)	138.3(6)	140.7(5)	126.8(5)	126.9(5)	132.8(3)	13.2(2)	3.89(1)	8.70(1)	8.386(8)	2.914(7)	2.252(6)
6.63(3)	137.3(6)	138.6(5)	126.4(5)	126.8(5)	133.0(3)	14.3(2)	3.87(1)	8.636(9)	8.379(8)	2.932(7)	2.219(6)
					Vishnevite (Lotti 2014)						
0.0001	153.0(7)	147.6(6)	139.9(6)	141.2(6)	152.5(4)	10.2(2)	4.025(12)	8.943(7)	8.750(8)	$2.942(6)^{Na1}$ $2.901(4)^{Na2}$	$2.465(7)^{Na1}$ $2.365(5)^{Na2}$
0.52(2)	151.9(9)	149.1(6)	138.3(9)	137.2(8)	147.5(5)	9.0(2)	4.01(2)	8.978(13)	8.725(17)	$2.897(10)^{Na1}$ $2.859(9)^{Na2}$	$2.485(10)^{Na1}$ $2.388(7)^{Na2}$
1.20(3)	150.2(8)	148.6(6)	137.4(9)	136.0(9)	146.2(5)	9.3(2)	3.99(3)	8.913(14)	8.695(18)	$2.898(10)^{Na1}$ $2.865(9)^{Na2}$	$2.463(11)^{Na1}$ $2.375(7)^{Na2}$
1.78(5)	149.0(9)	146.8(7)	135.8(8)	136.0(9)	145.1(5)	10.0(3)	3.98(2)	8.874(15)	8.670(18)	$2.899(10)^{Na1}$ $2.866(10)^{Na2}$	$2.432(11)^{Na1}$ $2.341(8)^{Na2}$
2.47(2)	147.8(10)	146.3(7)	135.5(9)	136.2(8)	144.8(5)	10.3(3)	3.96(2)	8.816(15)	8.642(18)	$2.892(12)^{Na1}$ $2.868(10)^{Na2}$	$2.402(17)^{Na1}$ $2.327(10)^{Na2}$
3.24(9)	147.4(9)	144.3(7)	132.6(8)	132.6(8)	141.5(5)	10.8(3)	3.98(2)	8.768(14)	8.558(16)	$2.903(11)^{Na1}$ $2.858(9)^{Na2}$	$2.408(15)^{Na1}$ $2.304(9)^{Na2}$

3.43(4)	145.0(8)	145.9(7)	134.4(8)	133.5(7)	141.5(5)	10.5(2)	3.93(2)	8.737(15)	8.594(17)	$2.889(10)^{Na1}$ $2.861(9)^{Na2}$	$2.401(13)^{Na1}$ $2.316(9)^{Na2}$
4.23(7)	143.1(8)	144.5(7)	131.5(7)	130.0(7)	137.7(4)	11.4(3)	3.92(2)	8.596(13)	8.513(15)	$2.905(9)^{Na1}$ $2.881(9)^{Na2}$	$2.367(11)^{Na1}$ $2.274(9)^{Na2}$
5.74(6)	142.5(9)	143.4(7)	128.9(7)	130.7(7)	136.0(4)	12.4(3)	3.90(2)	8.506(15)	8.493(17)	$2.943(10)^{Na1}$ $2.901(10)^{Na2}$	$2.371(12)^{Na1}$ $2.244(9)^{Na2}$
6.10(8)	143.3(9)	142.6(7)	128.0(8)	129.5(8)	135.0(5)	12.7(3)	3.87(3)	8.449(15)	8.473(18)	$2.956(11)^{Na1}$ $2.900(9)^{Na2}$	$2.367(13)^{Na1}$ $2.229(9)^{Na2}$
6.11(4)	138.9(9)	140.0(7)	128.4(8)	128.3(8)	135.3(5)	14.4(3)	3.84(3)	8.260(16)	8.43(2)	$2.984(11)^{Na1}$ $2.956(10)^{Na2}$	$2.290(14)^{Na1}$ $2.173(9)^{Na2}$
7.40(4)	136.2(10)	130.0(7)	125.1(13)	125.2(14)	129.9(10)	17.5(4)	3.71(3)	8.18(2)	8.916(16)	$2.942(12)^{Na1}$ $2.96(2)^{Na2}$	$2.078(17)^{Na1}$ $2.008(15)^{Na2}$

Balliranoite (Lotti et al. 2014b)

0.0001	155.4(3)	160.3(3)	136.1(4)	137.9(4)	161.4(2)	1.2(1)	4.400(10)	9.400(7)	8.279(11)	2.614(4)	2.560(4)
0.85(3)	152.9(3)	160.2(3)	133.7(4)	136.4(5)	157.7(2)	1.4(1)	4.399(10)	9.323(8)	8.202(11)	2.610(5)	2.551(4)
1.73(3)	150.3(3)	159.4(3)	132.5(4)	134.7(4)	154.4(2)	1.8(1)	4.392(10)	9.255(8)	8.173(10)	2.623(4)	2.544(4)
2.62(4)	148.4(3)	159.4(3)	131.7(4)	133.3(4)	152.8(2)	1.9(1)	4.390(10)	9.189(8)	8.120(11)	2.624(4)	2.542(4)
3.80(5)	146.4(3)	158.5(3)	130.5(4)	131.6(4)	148.8(2)	2.4(1)	4.357(10)	9.087(8)	8.077(9)	2.631(5)	2.525(4)
4.95(3)	144.6(3)	159.3(3)	129.0(4)	130.2(4)	146.9(2)	2.3(2)	4.354(11)	9.008(8)	8.015(11)	2.632(5)	2.536(4)
4.95(4)	143.6(3)	157.9(4)	128.6(5)	128.5(5)	145.3(3)	2.7(2)	4.333(12)	8.940(10)	7.964(13)	2.626(7)	2.513(5)
6.77(2)	142.3(3)	156.7(3)	127.5(4)	128.1(4)	143.8(2)	2.9(2)	4.339(10)	8.927(8)	7.947(11)	2.625(6)	2.504(5)

Davyne (Lotti et al. 2014a)

0.0001*	167.7(3)	158.1(3)	142.0(2)	-	180	2.5(1)	4.361(6)	9.451(6)	8.439(4)	2.661(4)	2.533(4)
0.38(2)	169.1(6)	157.1(4)	139.9(5)	142.6(5)	170.1(4)	3.0(2)	4.328(11)	9.414(11)	8.460(11)	$2.676(7)^{Ca1}$ $2.681(7)^{Ca2}$	$2.521(6)^{Ca1}$ $2.522(6)^{Ca2}$
0.91(3)	164.2(6)	157.6(4)	140.1(5)	139.9(5)	168.6(3)	2.9(2)	4.344(8)	9.377(10)	8.403(8)	$2.680(7)^{Ca1}$ $2.672(7)^{Ca2}$	$2.517(5)^{Ca1}$ $2.532(6)^{Ca2}$
1.57(5)	159.3(6)	156.2(4)	139.0(4)	138.2(4)	162.6(3)	3.6(2)	4.325(8)	9.301(9)	8.373(8)	$2.683(7)^{Ca1}$ $2.680(7)^{Ca2}$	$2.490(5)^{Ca1}$ $2.510(6)^{Ca2}$
2.05(6)	157.5(5)	156.7(4)	137.3(4)	137.7(4)	160.8(2)	3.4(2)	4.328(7)	9.280(9)	8.329(7)	$2.700(7)^{Ca1}$ $2.668(7)^{Ca2}$	$2.487(5)^{Ca1}$ $2.513(6)^{Ca2}$

3.07(2)	154.6(5)	155.2(4)	134.5(3)	137.2(4)	157.3(2)	4.0(2)	4.327(11)	9.192(9)	8.264(7)	$2.674(7)^{Ca1}$ $2.674(7)^{Ca2}$	$2.462(5)^{Ca1}$ $2.491(6)^{Ca2}$
3.49(2)	153.4(5)	156.0(4)	134.4(3)	137.0(3)	156.2(2)	3.5(2)	4.304(11)	9.187(8)	8.254(7)	$2.655(5)^{Ca1}$ $2.656(7)^{Ca2}$	$2.473(5)^{Ca1}$ $2.495(6)^{Ca2}$
4.56(7)	151.1(6)	155.7(5)	132.9(4)	136.0(4)	153.2(2)	3.6(2)	4.287(14)	9.129(9)	8.207(8)	$2.649(7)^{Ca1}$ $2.650(7)^{Ca2}$	$2.460(6)^{Ca1}$ $2.490(7)^{Ca2}$
5.33(8)	149.9(6)	156.2(5)	131.7(4)	134.4(4)	152.0(3)	3.6(2)	4.293(14)	9.064(9)	8.160(8)	$2.656(6)^{Ca1}$ $2.658(7)^{Ca2}$	$2.470(6)^{Ca1}$ $2.505(7)^{Ca2}$
6.10(8)	148.8(7)	155.6(5)	129.9(4)	133.8(4)	150.2(3)	3.9(2)	4.290(15)	9.011(9)	8.113(9)	$2.655(6)^{Ca1}$ $2.659(6)^{Ca2}$	$2.455(6)^{Ca1}$ $2.494(7)^{Ca2}$
7.18(6)	148.0(7)	155.1(6)	129.2(5)	133.3(5)	147.9(3)	4.1(2)	4.254(16)	8.953(11)	8.090(10)	$2.647(8)^{Ca1}$ $2.655(8)^{Ca2}$	$2.443(8)^{Ca1}$ $2.483(9)^{Ca2}$

$\alpha_{S6R\perp[0001]} = \Sigma_i\{1/6\cdot[|120°-\theta_i|/2]\}$ (see Figure 6; parameter originally defined for phyllosilicates, Brigatti and Guggenheim 2002)
* $P6_3/m$ davyne sample at 0.0001 GPa, $P6_3$ davyne at all the other pressures (Lotti et al. 2014a).

801

802 **Table 4 (deposited).** Relevant inter-tetrahedral angles (°), voids diameters (Å), bond distances (Å) and the ditrigonal rotation angle (°) at different
803 temperatures of cancrinite-group minerals.

T (K)	Si-O1-Al	Si-O2-Al	Si-O3-Al	Si-O4-Al	O3-O4-O3	$\alpha_{S6R\perp[0001]}$	O3-O4$_{S4R}$	O1-O1$_{12R}$	O3-O4$_{12R}$	(Na,Ca)-O1	(Na,Ca)-O2
					Cancrinite (Hassan et al. 2006)						
298	151.6(6)	155.3(5)	142.7(10)	125.2(9)	146.8*	7.63*	4.160*	8.793*	8.447*	2.888(7)	2.521(6)
374	152.2(6)	155.5(5)	142.8(10)	126.1(9)	147.8*	7.18*	4.157*	8.814*	8.457*	2.881(7)	2.524(6)
480	152.7(6)	155.8(5)	142.3(11)	127.2(11)	148.8*	7.08*	4.167*	8.845*	8.461*	2.871(7)	2.531(6)
571	152.8(6)	156.3(5)	140.5(12)	129.9(13)	150.9*	6.70*	4.186*	8.884*	8.456*	2.861(6)	2.543(6)
678	152.9(6)	156.7(4)	138.4(14)	135.3(16)	154.0*	6.40*	4.189*	8.931*	8.465*	2.850(7)	2.567(5)
769	153.7(6)	157.8(4)	139.2(11)	134.1(11)	154.7*	5.98*	4.189*	8.953*	8.486*	2.852(7)	2.587(5)
784	153.4(6)	157.6(4)	139.0(10)	134.0(11)	154.6*	5.95*	4.186*	8.959*	8.487*	2.847(7)	2.586(5)
830	152.2(6)	158.3(4)	140.3(9)	132.5(9)	154.3*	6.05*	4.206*	8.941*	8.478*	2.857(7)	2.596(5)
875	151.0(6)	157.8(4)	140.1(10)	132.9(10)	154.3*	5.90*	4.202*	8.989*	8.490*	2.838(7)	2.593(5)
921	151.8(6)	158.4(4)	140.1(9)	132.4(10)	155.3*	5.90*	4.229*	8.971*	8.474*	2.851(7)	2.599(5)
966	152.4(6)	158.9(4)	139.6(9)	132.7(10)	155.7*	5.78*	4.242*	8.973*	8.468*	2.852(7)	2.603(5)
1073	155.1(7)	158.7(5)	138.6(9)	133.2(10)	157.7*	5.75*	4.256*	8.972*	8.470*	2.866(7)	2.604(6)
1164	156.1(7)	159.5(5)	139.8(11)	133.5(11)	159.9*	5.60*	4.285*	8.976*	8.461*	2.876(8)	2.622(6)
1225	154.5(10)	160.6(6)	141.0(16)	134.7(15)	162.9*	4.78*	4.270*	9.052*	8.499*	2.837(9)	2.639(8)
					Cancrinite (Isupova et al. 2010)						
173	146.4(1)	151.1(1)	133.2(2)	133.18(8)	144.9*	9.03*	4.134*	8.800*	8.475*	2.877(2)	2.429(2)
293	147.4(1)	151.86(9)	133.8(2)	133.71(7)	145.7*	8.43*	4.144*	8.856*	8.493*	2.866(2)	2.444(2)
473	149.8(2)	153.2(2)	135.1(2)	135.0(2)	149.2*	7.73*	4.163*	8.923*	8.502*	2.854(2)	2.469(3)
673	151.5(2)	152.2(2)	136.6(2)	136.2(2)	151.5*	7.95*	4.146*	8.950*	8.540*	2.857(3)	2.461(4)
					Cancrinite (Gatta et al. 2014)						
303	147.2(2)	151.2(2)	133.4(2)	133.3(2)	144.6(3)	8.48(9)	4.145(6)	8.862(5)	8.487(4)	2.862(3)	2.437(4)
478	148.0(2)	152.5(2)	134.0(2)	134.1(2)	146.39(16)	7.99(8)	4.166(6)	8.901(5)	8.485(4)	2.854(2)	2.455(3)

748	151.2(3)	151.0(3)	136.1(3)	136.6(3)	149.8(2)	8.19(12)	4.155(8)	8.971(7)	8.536(5)	2.846(3)	2.446(4)

Cancrinite (Gatta et al. 2012a)

293	147.02(9)	151.79(7)	133.46(7)	133.55(7)	144.84(2)	8.45(3)	4.129(3)	8.841(2)	8.486(1)	2.858(1)	2.437(1)
250	146.46(8)	151.45(10)	133.26(7)	133.26(7)	144.42(5)	8.66(3)	4.123(2)	8.815(2)	8.471(1)	2.863(1)	2.429(1)
220	146.14(8)	151.27(10)	133.05(6)	133.02(6)	143.98(4)	8.75(3)	4.120(2)	8.810(2)	8.475(1)	2.866(1)	2.427(1)
180	145.85(8)	150.90(9)	132.83(7)	132.85(7)	143.71(5)	8.87(3)	4.117(2)	8.802(2)	8.472(1)	2.866(1)	2.421(1)
140	145.42(8)	150.74(9)	132.78(7)	132.72(7)	143.37(5)	9.05(3)	4.111(2)	8.783(2)	8.474(1)	2.873(1)	2.418(1)
100	145.32(7)	150.56(9)	132.55(7)	132.66(7)	143.05(5)	9.09(3)	4.108(2)	8.783(1)	8.480(1)	2.875(1)	2.416(1)

Vishnevite (Lotti 2014)

293	153.3(2)	147.4(3)	140.6(4)	140.2(4)	152.6(2)	10.2(1)	4.042(10)	8.930(5)	8.726(7)	2.920(3)	2.411(4)
110	151.6(2)	146.8(2)	139.6(4)	139.4(4)	151.2(2)	10.8(1)	4.015(10)	8.852(5)	8.715(6)	2.937(3)	2.400(4)

Balliranoite (Gatta et al. 2013b)

293	155.98(8)	161.28(6)	136.44(6)	137.33(7)	162.68(5)	1.02(3)	4.427(1)	9.387(1)	8.251(2)	2.6218(9)	2.5761(8)
250	155.27(8)	161.28(7)	136.13(6)	137.09(6)	161.81(4)	1.03(3)	4.424(1)	9.373(2)	8.239(2)	2.620(1)	2.5752(9)
220	154.81(7)	161.21(6)	135.98(6)	136.84(6)	161.43(4)	1.04(3)	4.430(1)	9.372(2)	8.235(2)	2.6207(9)	2.5753(8)
180	154.32(8)	161.17(6)	135.70(6)	136.65(6)	160.85(4)	1.07(3)	4.428(1)	9.367(2)	8.231(2)	2.6209(9)	2.5746(9)
140	153.92(8)	161.23(7)	135.51(6)	136.42(6)	160.43(4)	1.06(6)	4.427(1)	9.356(2)	8.219(2)	2.619(1)	2.5738(9)
108	153.65(8)	161.21(7)	135.40(6)	136.29(7)	160.18(4)	1.08(3)	4.429(1)	9.352(6)	8.215(2)	2.620(1)	2.5741(9)

Davyne (Gatta et al. 2013a)

293	166.15(7)	156.87(5)	141.83(7)	141.52(6)	171.51(4)	3.00(2)	4.331(2)	9.427(1)	8.467(1)	2.6715(8)	2.5162(7)
250	164.87(6)	156.96(5)	141.85(6)	141.24(5)	169.96(4)	3.00(2)	4.323(2)	9.413(1)	8.460(1)	2.6701(7)	2.5153(7)
220	164.02(5)	156.80(4)	141.43(5)	141.06(4)	169.00(3)	3.00(2)	4.327(1)	9.412(1)	8.4512(8)	2.6675(6)	2.5129(6)
180	163.05(5)	156.88(4)	141.24(5)	140.73(4)	167.92(3)	3.00(2)	4.327(1)	9.404(1)	8.4459(8)	2.6685(6)	2.5140(6)
140	162.45(5)	156.77(4)	141.05(5)	140.29(4)	167.22(3)	3.02(2)	4.331(1)	9.400(1)	8.4357(8)	2.6670(6)	2.5121(6)
110	161.99(5)	156.73(4)	140.86(5)	140.26(4)	166.65(3)	3.04(2)	4.329(1)	9.394(1)	8.4334(8)	2.6677(6)	2.5117(6)

Pitiglianoite** (Bonaccorsi et al. 2007)

298	155.9(4)	144.9(4)	143.2(4)	144.0(4)	155.7*	11.25*	4.000*	8.953*	8.835*	$2.954(5)^{Na}$	$2.394(6)^{Na}$
730	152.7(5)	147.9(6)	139.3(6)	139.6(7)	152.0*	10.03*	4.051*	8.942*	8.730*	$2.917(9)^{Na}$	$2.42(1)^{Na}$ $2.82(1)^{K}$
298 post-H*T*	147.9(3)	148.0(2)	136.8(2)	136.5(2)	147.6*	10.00*	4.078*	8.868*	8.646*	$2.911(4)^{Na}$ $3.122(4)^{K}$	$2.397(8)^{Na}$ $2.760(5)^{K}$

$\alpha_{S6R\perp[0001]} = \Sigma_i\{1/6\cdot[|120°-\theta_i|/2]\}$ (see Figure 6; parameter originally defined for phyllosilicates, Brigatti and Guggenheim 2002)
*Calculated from published data; ** Structure refinements performed in the vishnevite subcell.

804

Figures Captions

Figure 1. *(Top left)* The hexagonal array of single six-membered rings of tetrahedra in the plane perpendicular to the **c**-axis (S6R⊥[0001]). (*Top right*) A portion of a column of *can* units. Two base-sharing cages are shown, along with a portion of a *dzc* chain. *(Bottom left)* The [CAN] framework viewed down [0001] of davyne and *(bottom right)* cancrinite. The S6R⊥[0001] cage-bases, the large 12R-channel and the S4R-units are shown.

Figure 2. (*Top*) Schematic view of the Na-H_2O and Ca-Cl chains in the columns of *can* units of cancrinite- and davyne-subgroup minerals, respectively. (*Bottom*) Cage-Na^+ (*left side*) and cage-Ca^{2+} (*right side*) coordination environments in cancrinite and davyne, respectively. Dashed lines represent mutually exclusive bonds.

Figure 3. (*Left side*) Schematic view (down the **c**-axis) of the extraframework population in the channels of cancrinite-group minerals, showing the cationic sites (C), close to the channel walls, and the anions/molecules positions, at the center of the channel. (*Middle***)** Coordination shell of the (Na^+,Ca^{2+}) cations in the channels of cancrinite and balliranoite. (*Right side*) The two possible and mutually exclusive configurations of the channel population in vishnevite and davyne: the SO_4^{2-} group can coexist with an "external" Na site at the same *z* coordinate, but it is mutually exclusive with the "internal" K site. If the maximum content of one SO_4^{2-} per formula unit is reached, the channel must be internally ordered. The potential upward and downward configurations of the SO_4^{2-} tetrahedra are shown. Dashed lines represent mutually exclusive bonds.

Figure 4. The pressure-induced evolution of the unit cell volume, and *a* and *c* cell edges of cancrinite (Lotti et al. 2012), vishnevite (Lotti 2014), balliranoite (Lotti et al. 2014b) and davyne (Lotti et al. 2014a).

Figure 5. The inter-tetrahedral O3-O4-O3 angle in $P6_3$ davyne (*left side*) is symmetry-induced to O3-O3-O3 = 180° in $P6_3/m$ davyne (*right side*), for the presence of mirror planes at $z = 0.25$ and 0.75.

Figure 6. The [CAN] framework of cancrinite viewed down [0001] (*left side*) and two base-sharing *can* units (*right side*) showing the relevant structural parameters (diameters and angles) reported in Tables 3 and 4.

Figure 7. The pressure-induced evolution of the inter-tetrahedral Si-O1-Al (squares), Si-O2-Al (circles), Si-O3-Al (triangles) and Si-O4-Al (diamonds) angles of cancrinite (Lotti et al. 2012), vishnevite (Lotti 2014), balliranoite (Lotti et al. 2014b) and davyne (Lotti et al. 2014a).

841 **Figure 1**. *(Top left)* The hexagonal array of single six-membered rings of tetrahedra in the plane
842 perpendicular to the **c**-axis (S6R⊥[0001]). (*Top right*) A portion of a column of *can* units. Two
843 base-sharing cages are shown, along with a portion of a *dzc* chain. *(Bottom left)* The [CAN]
844 framework viewed down [0001] of davyne and *(bottom right)* cancrinite. The S6R⊥[0001] cage-
845 bases, the large 12R-channel and the S4R-units are shown.

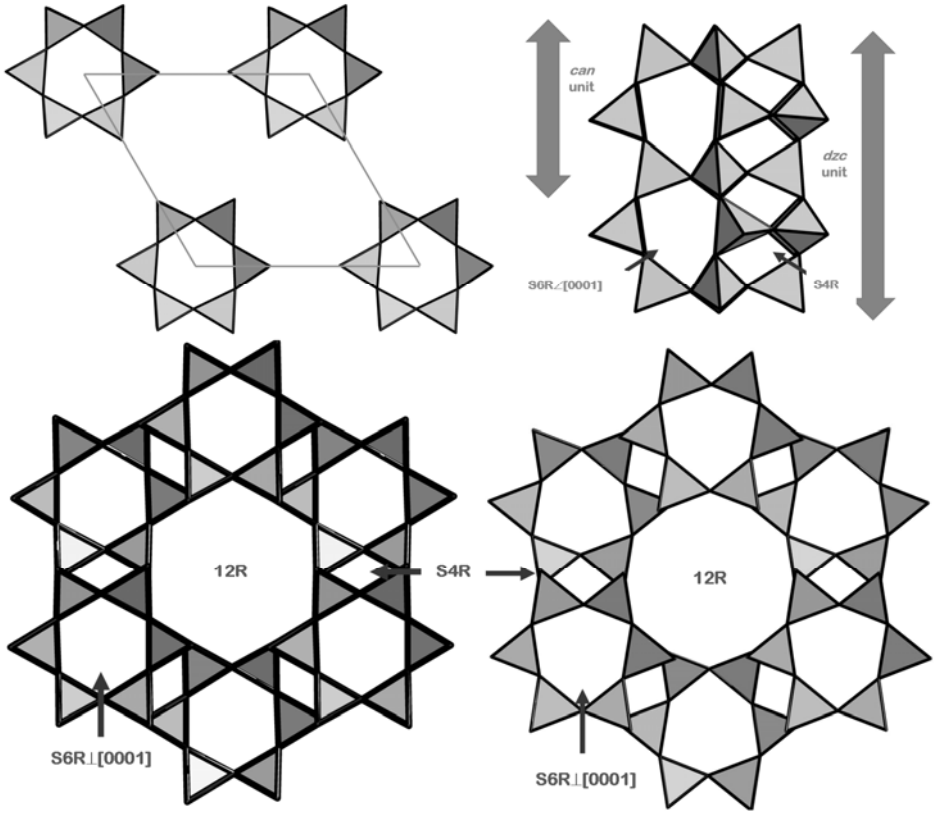

846

847

Figure 2. (*Top*) Schematic view of the Na-H_2O and Ca-Cl chains in the columns of *can* units of cancrinite- and davyne-subgroup minerals, respectively. (*Bottom*) Cage-Na^+ (*left side*) and cage-Ca^{2+} (*right side*) coordination environments in cancrinite and davyne, respectively. Dashed lines represent mutually exclusive bonds.

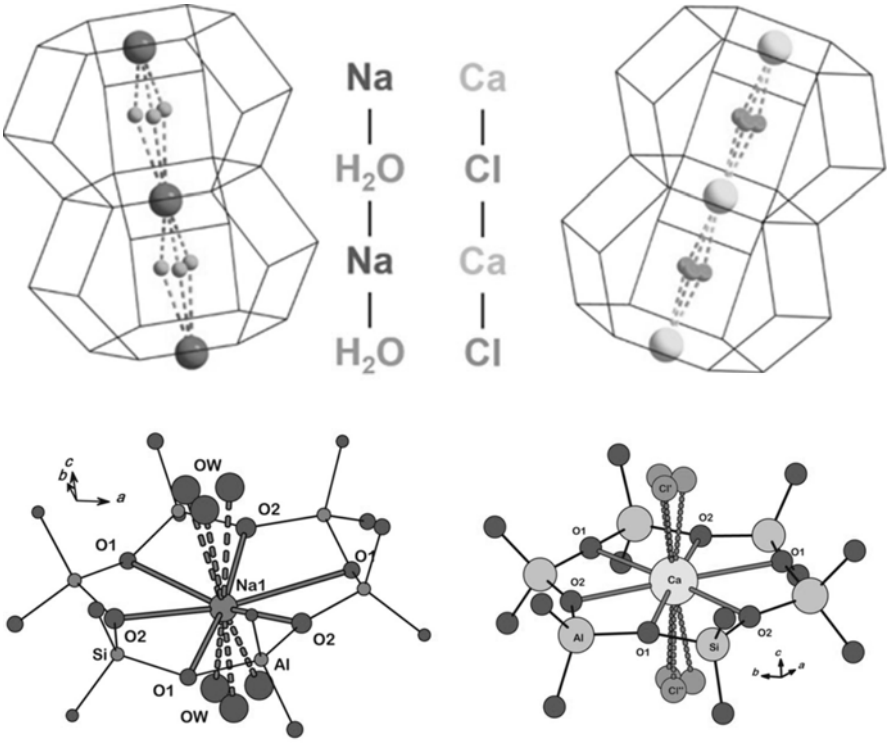

Figure 3. (*Left side*) Schematic view (down the **c**-axis) of the extraframework population in the channels of cancrinite-group minerals, showing the cationic sites (C), close to the channel walls, and the anions/molecules positions, at the center of the channel. (*Middle***)** Coordination shell of the (Na^{+},Ca^{2+}) cations in the channels of cancrinite and balliranoite. (*Right side*) The two possible and mutually exclusive configurations of the channel population in vishnevite and davyne: the SO_4^{2-} group can coexist with an "external" Na site at the same *z* coordinate, but it is mutually exclusive with the "internal" K site. If the maximum content of one SO_4^{2-} per formula unit is reached, the channel must be internally ordered. The potential upward and downward configurations of the SO_4^{2-} tetrahedra are shown. Dashed lines represent mutually exclusive bonds.

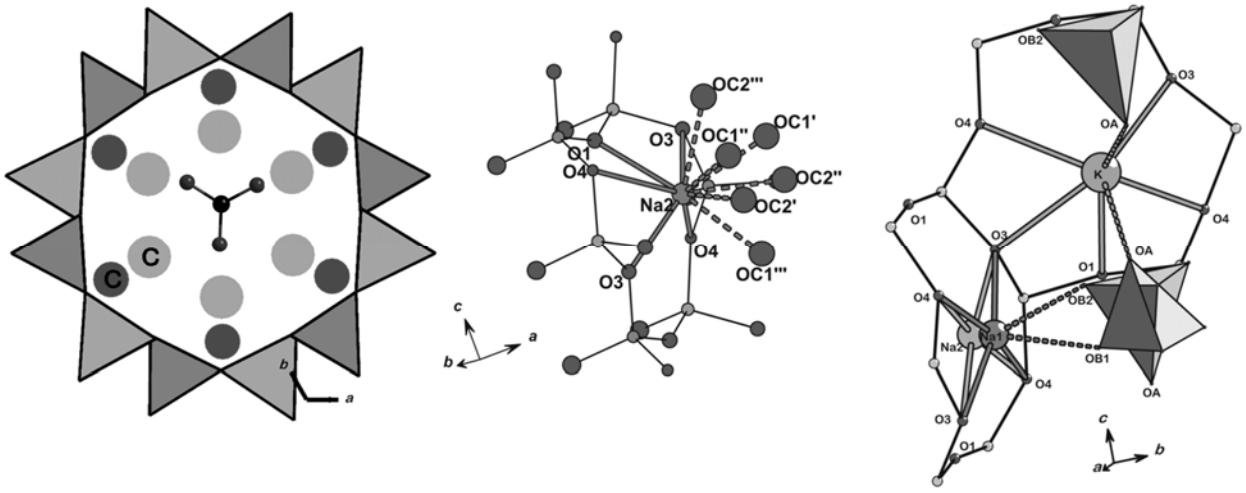

866 **Figure 4.** The pressure-induced evolution of the unit cell volume, and *a* and *c* cell edges of
867 cancrinite (Lotti et al. 2012), vishnevite (Lotti 2014), balliranoite (Lotti et al. 2014b) and davyne
868 (Lotti et al. 2014a).

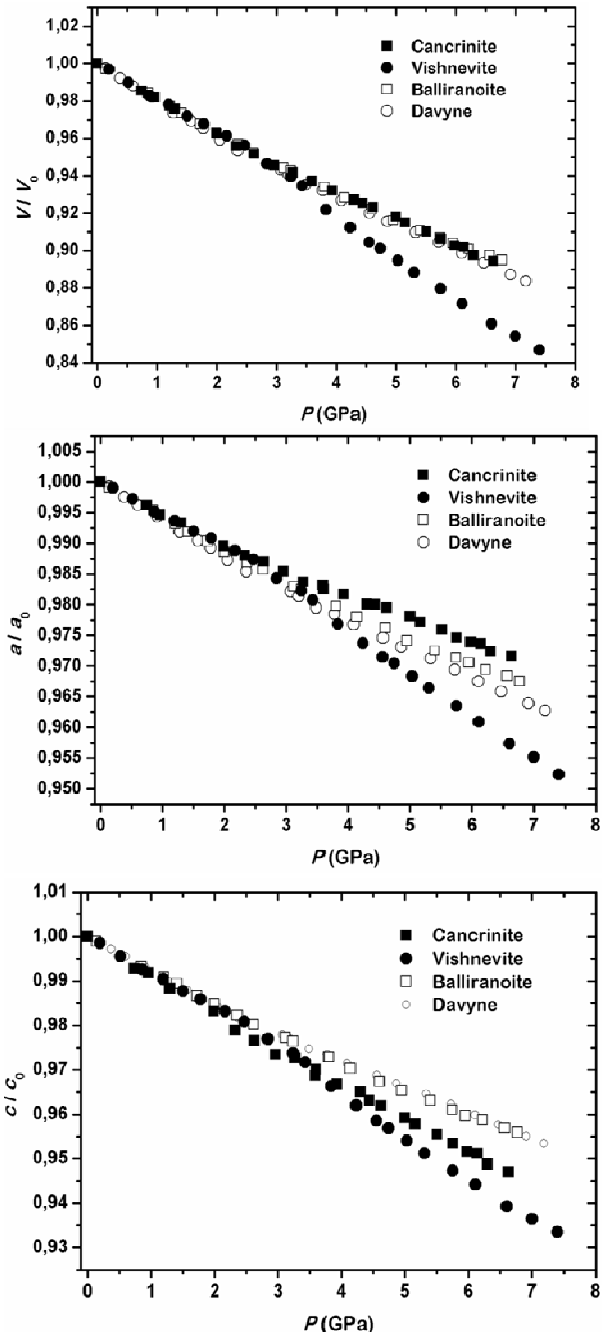

869

870

871 **Figure 5.** The inter-tetrahedral O3-O4-O3 angle in $P6_3$ davyne (*left side*) is symmetry-induced to
872 O3-O3-O3 = 180° in $P6_3/m$ davyne (*right side*), for the presence of mirror planes at z = 0.25 and
873 0.75.

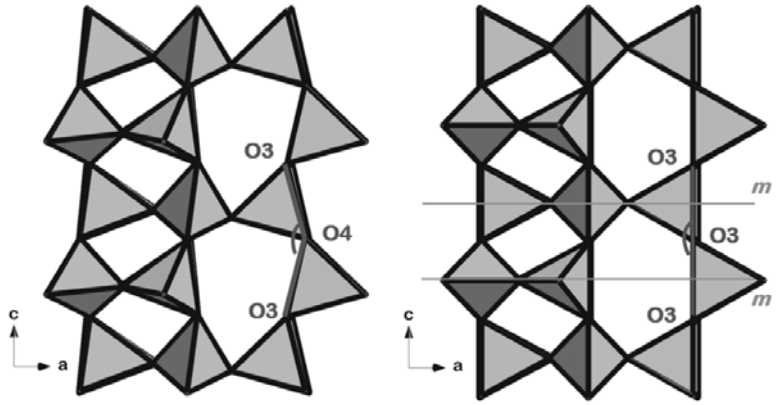

874

875

Figure 6. The [CAN] framework of cancrinite viewed down [0001] (*left side*) and two base-sharing *can* units (*right side*) showing the relevant structural parameters (diameters and angles) reported in Tables 3 and 4 (deposited).

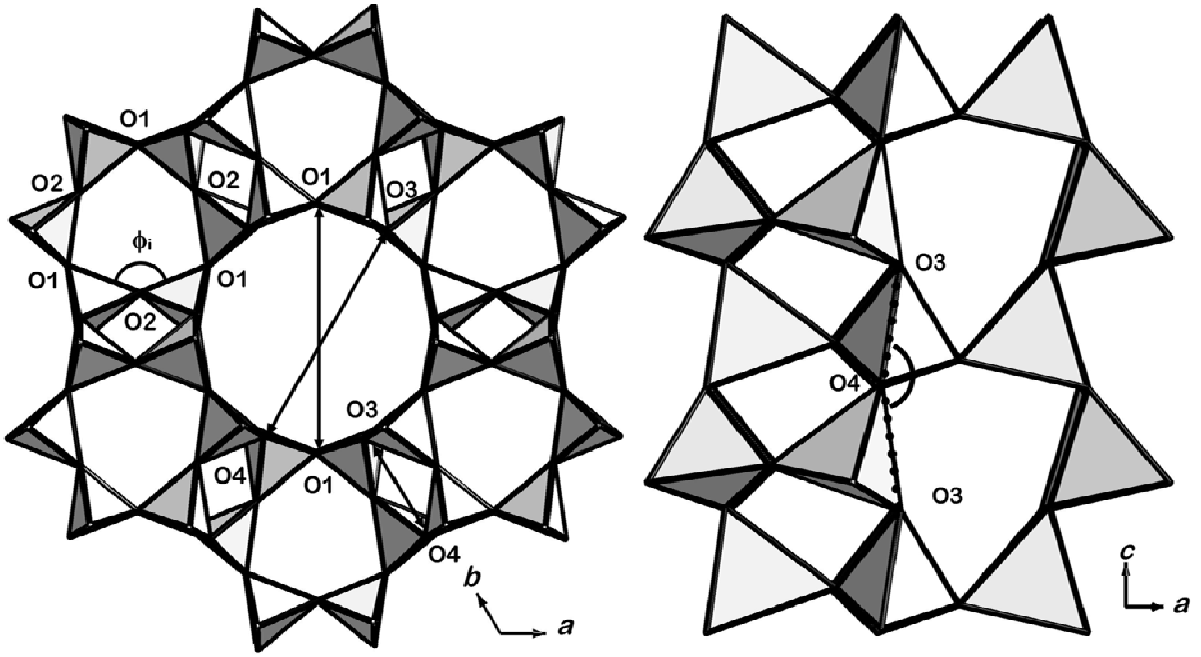

881 **Figure 7.** The pressure-induced evolution of the inter-tetrahedral Si-O1-Al (squares), Si-O2-Al
882 (circles), Si-O3-Al (triangles) and Si-O4-Al (diamonds) angles of cancrinite (Lotti et al. 2012),
883 vishnevite (Lotti 2014), balliranoite (Lotti et al. 2014b) and davyne (Lotti et al. 2014a).

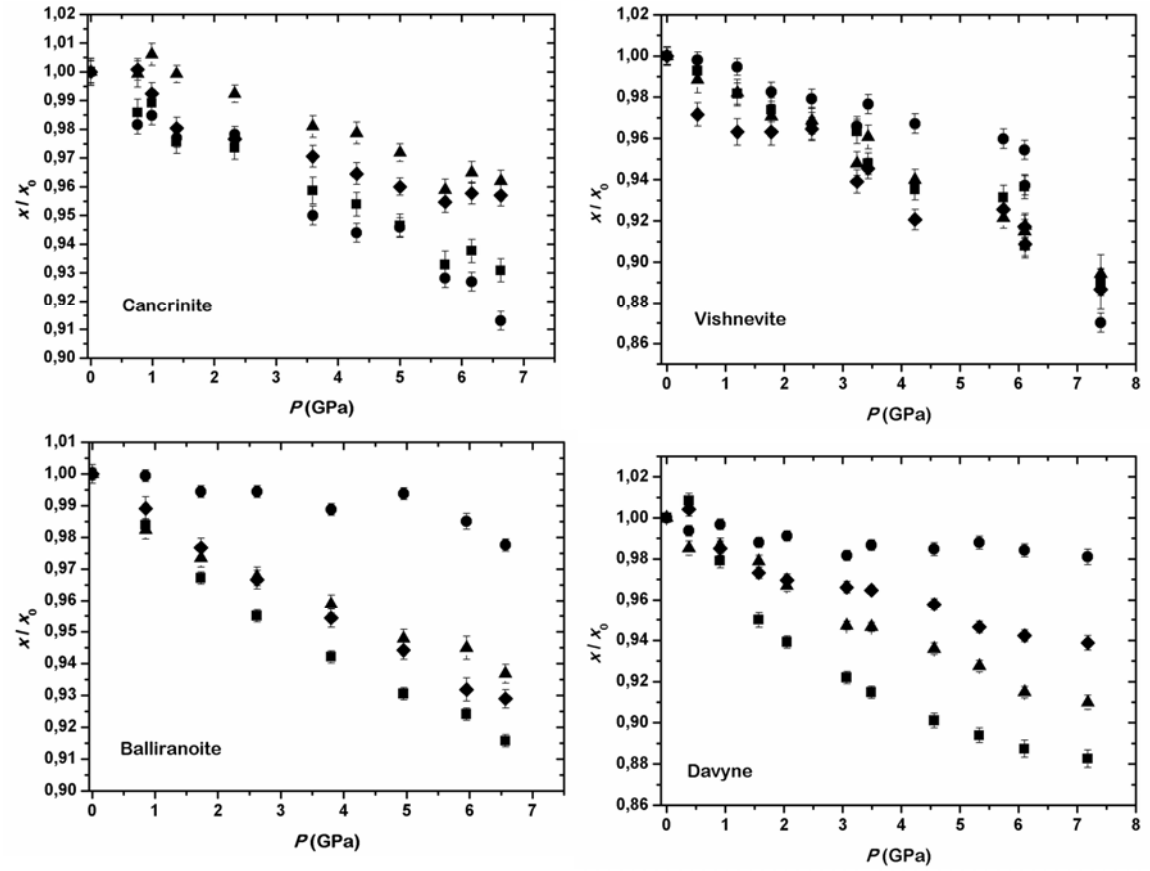

884

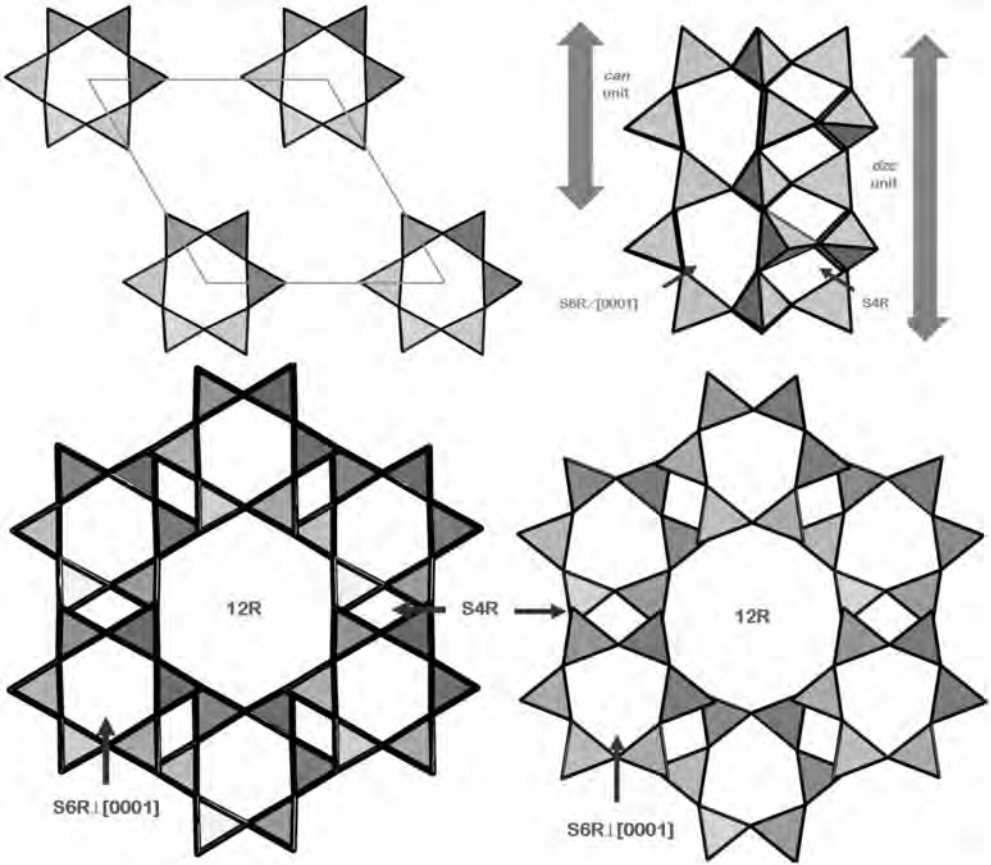
can
unit
dzc
unit
S8R⊥[0001]
S4R
12R
S4R
S6R⊥[0001]
12R
S6R⊥[0001]

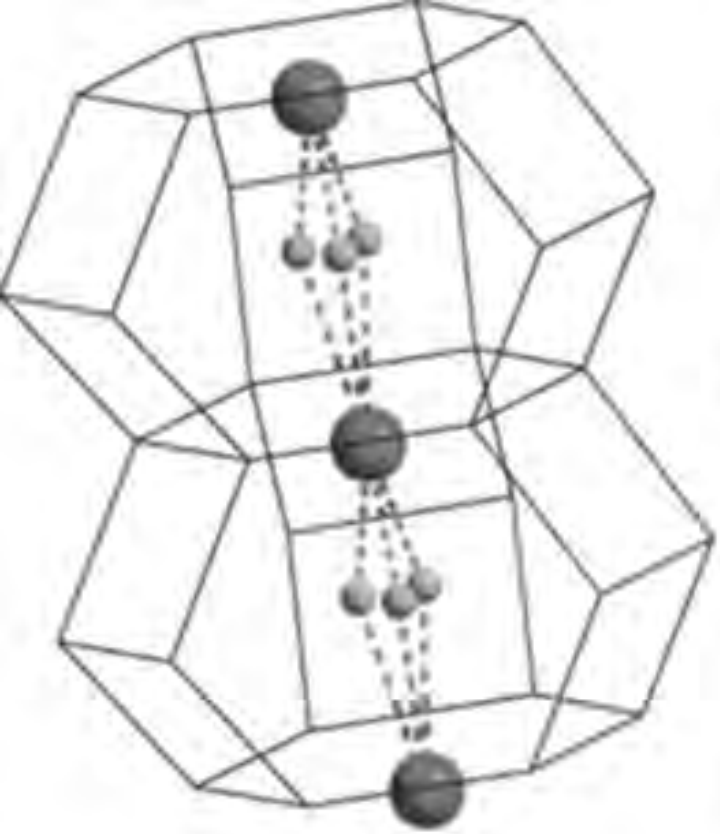

Na
Ca
H2O
Cl
Na
Ca
H2O
Cl

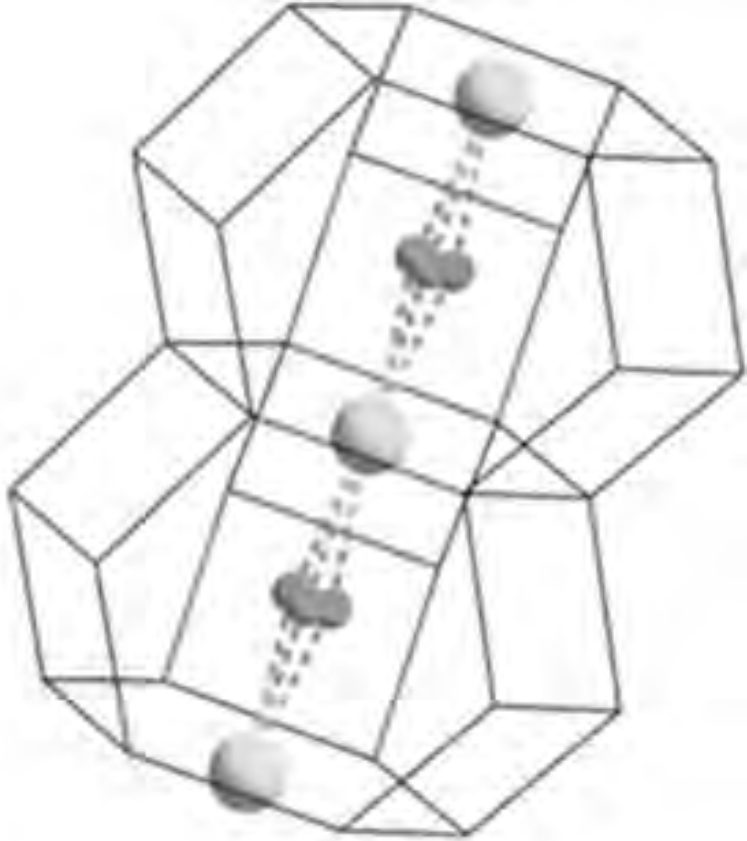

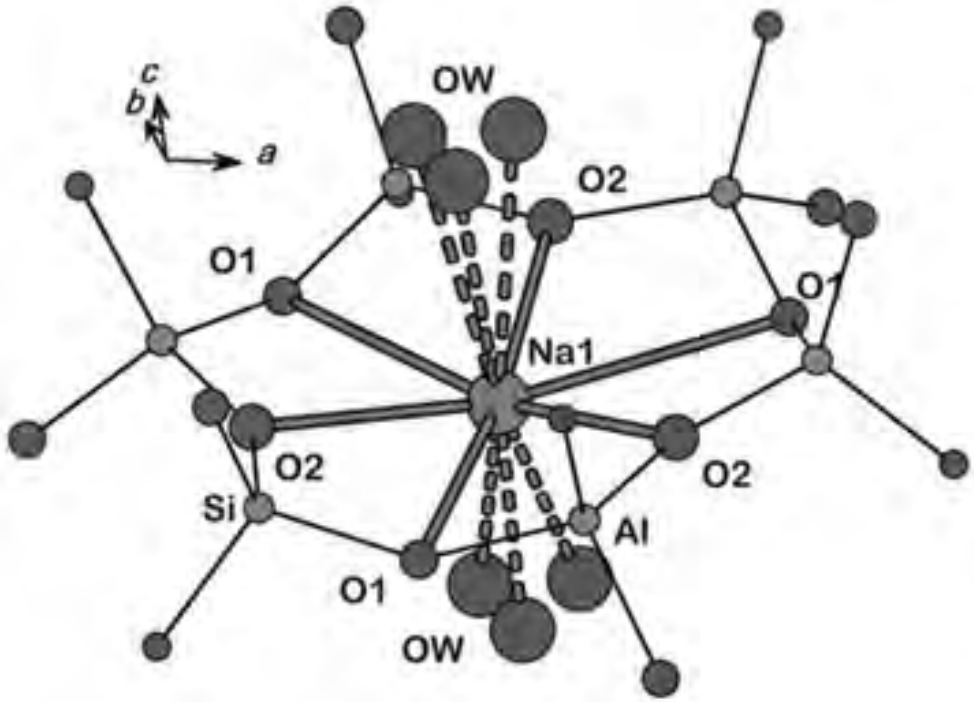
c
b
a
OW
O2
O1
O1
Na1
O2
O2
Si
Al
O1
OW

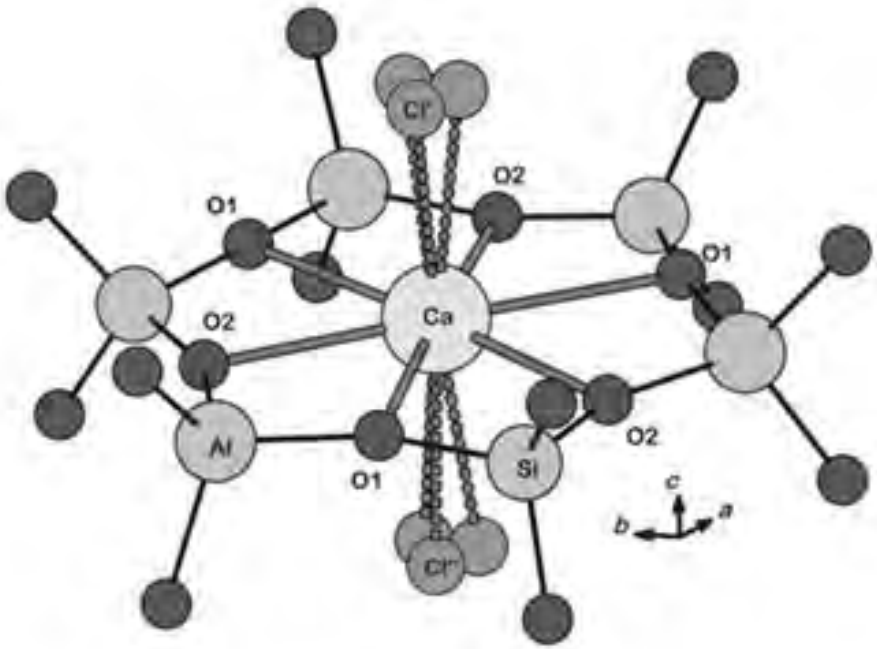
Cl
O2
O1
O1
Ca
O2
Al
O1
Si
O2
Cl
c
b
a

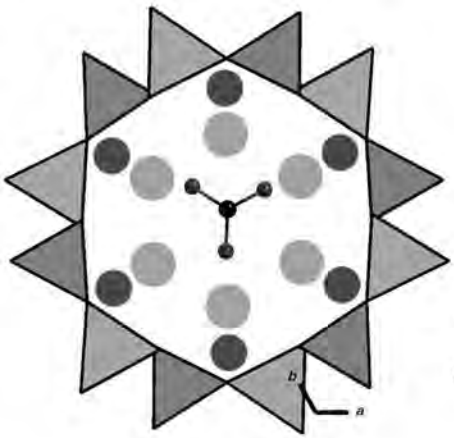
b
a

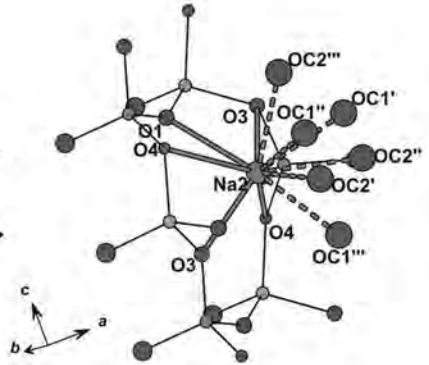
OC2'''
OC1''
OC1'
O3
O1
O4
OC2''
Na2
OC2'
O4
OC1'''
O3
c
a
b

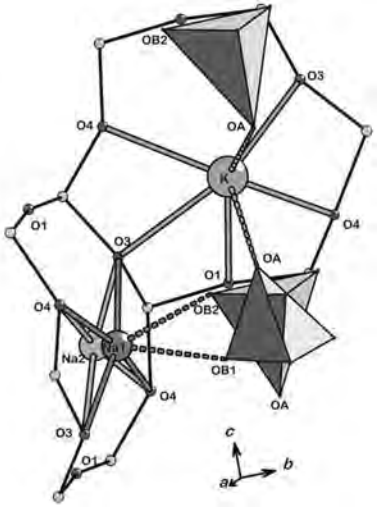
OB2
O3
O4
OA
K
O1
O4
O3
OA
O1
O4
OB2
Na2
Na1
OB1
O4
OA
O3
O1
c
b
a

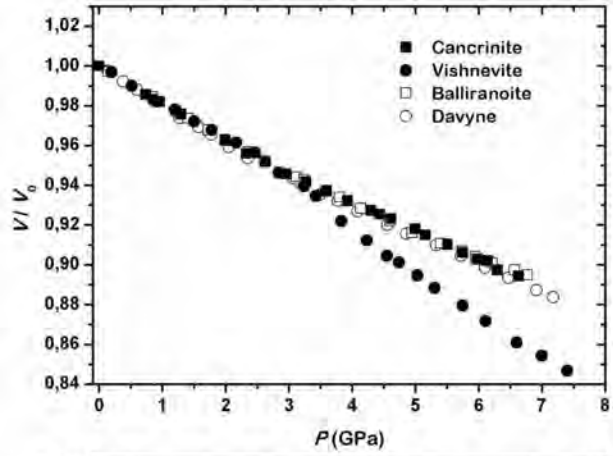
Cancrinite
Vishnevite
Balliranoite
Davyne
V / V0
P (GPa)

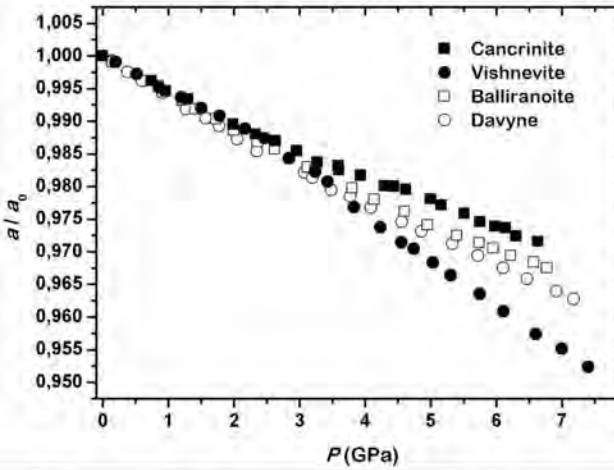
Cancrinite
Vishnevite
Balliranoite
Davyne
a / a0
P (GPa)

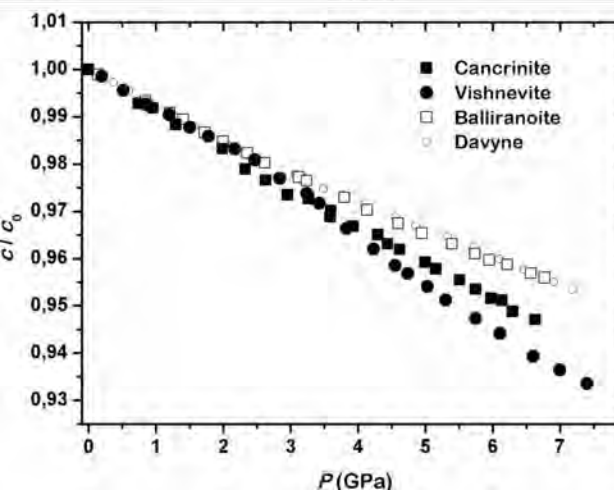
Cancrinite
Vishnevite
Balliranoite
Davyne
c / c0
P (GPa)

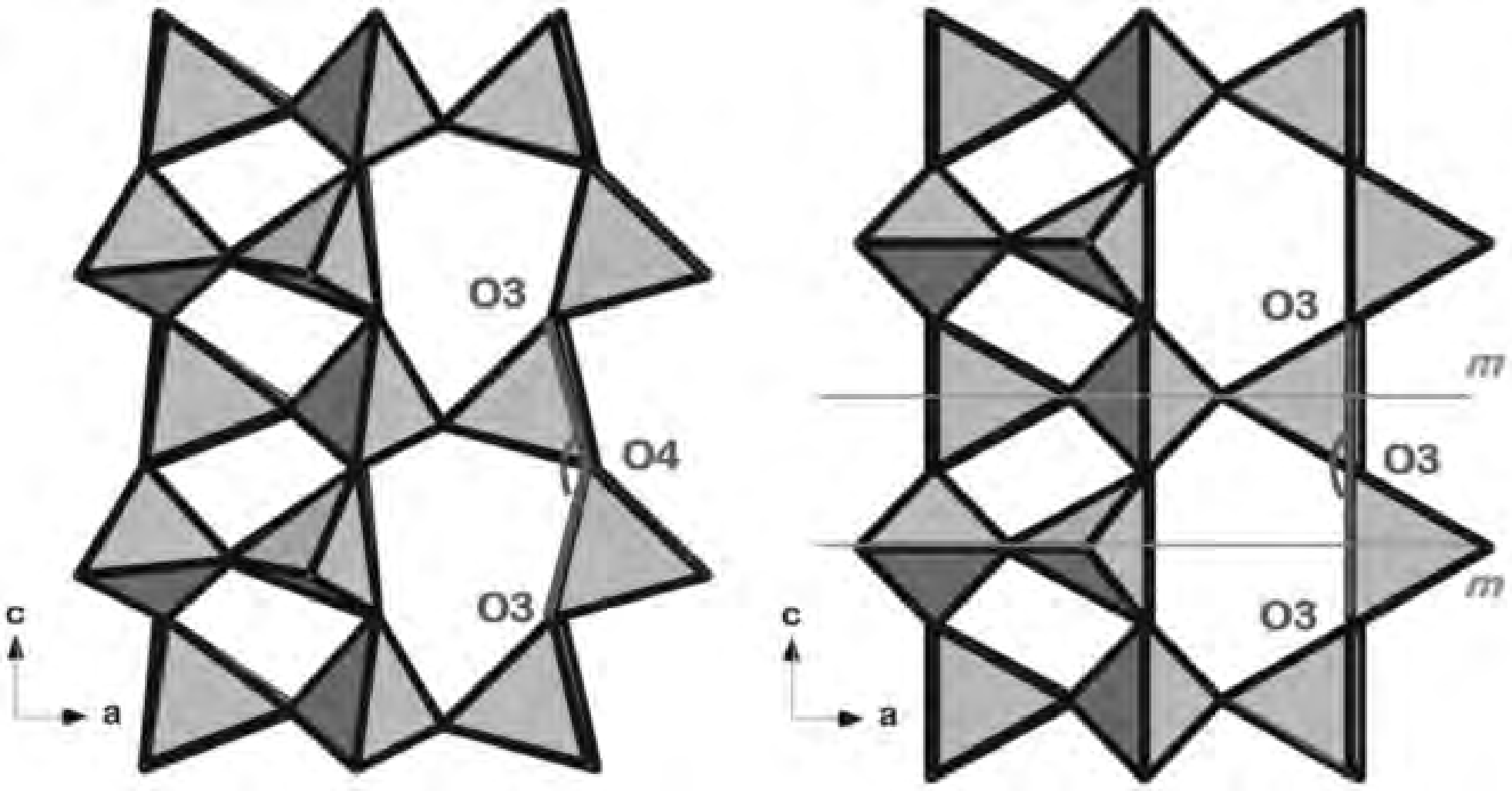
O3
O4
O3
c
a
O3
m
O3
m
O3
c
a

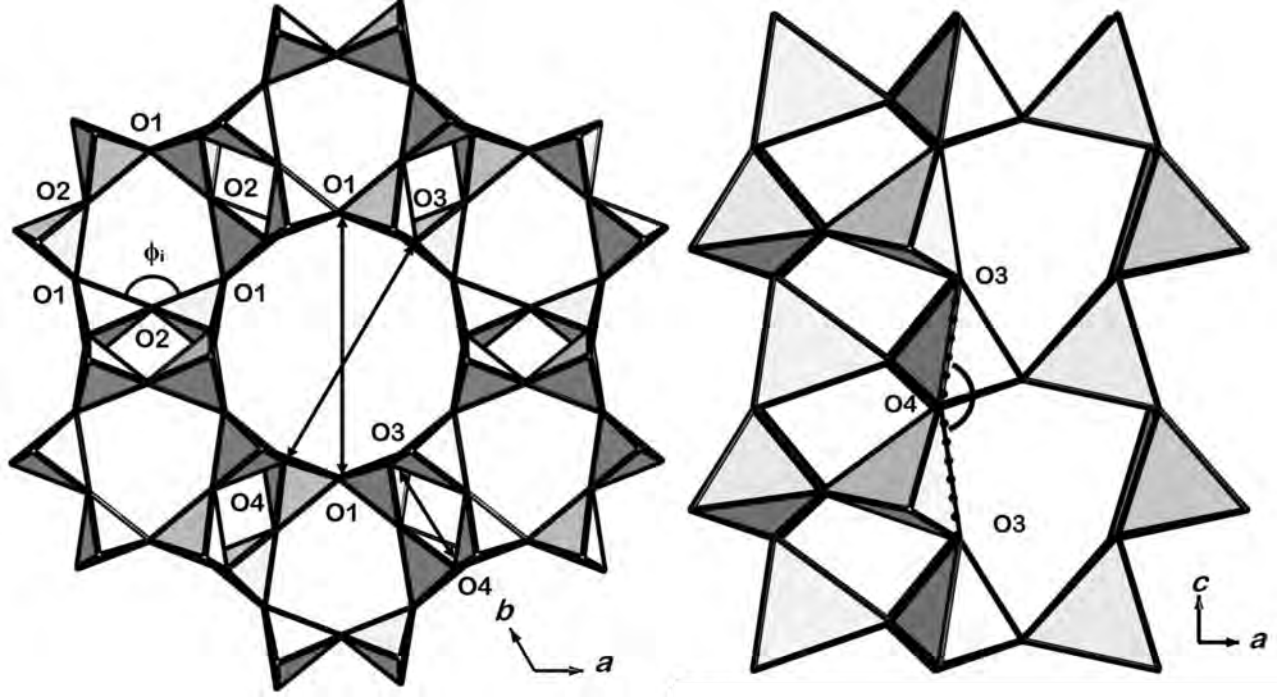
O1
O2
O2
O1
O3
ϕi
O1
O1
O2
O3
O4
O1
O4
b
a
O3
O4
O3
c
a

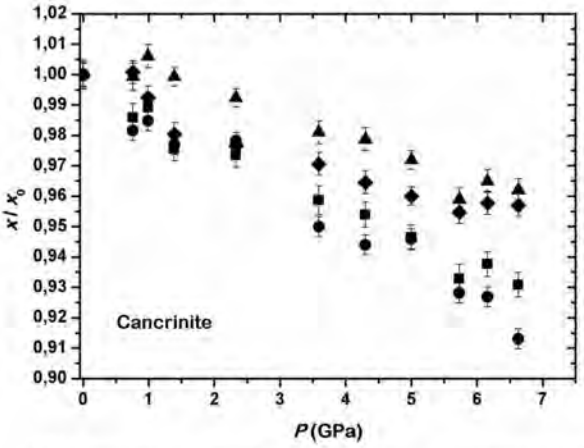
Cancrinite
X / X0
P (GPa)

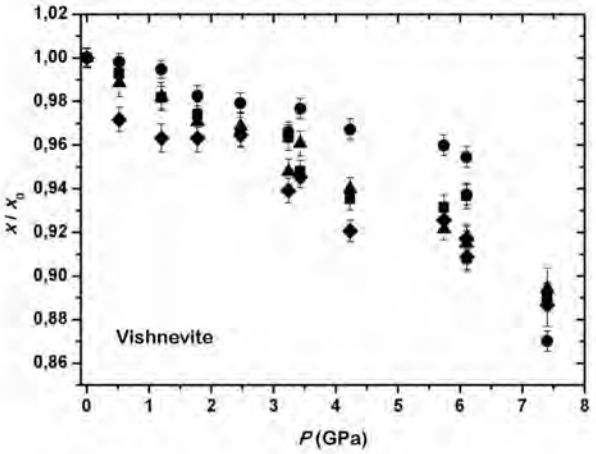
Vishnevite
X / X0
P (GPa)

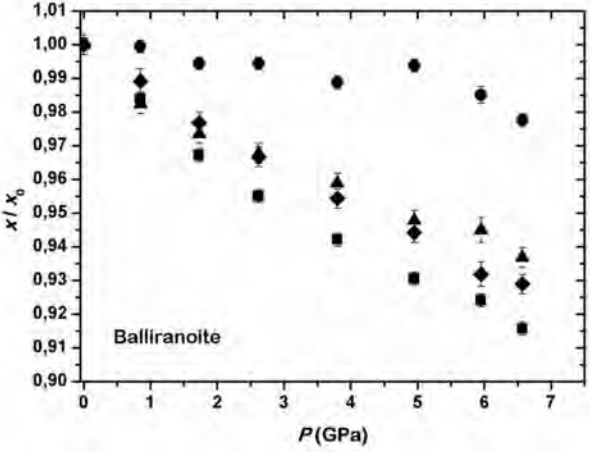
Balliranoite
X / X0
P (GPa)

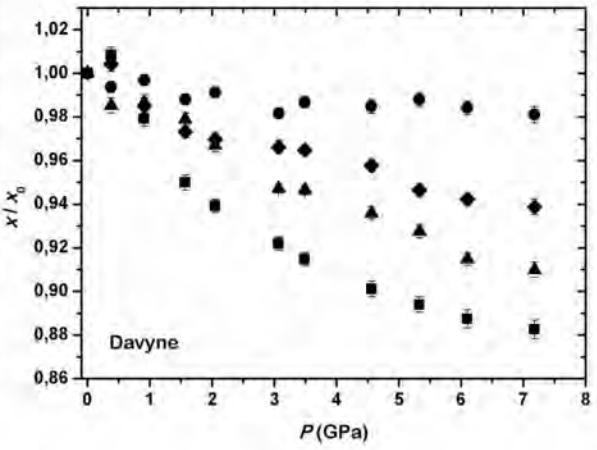
Davyne
X / X0
P (GPa)